DOI:10.14753/SE.2024.3041

SEMMELWEIS EGYETEM

DOKTORI ISKOLA

Ph.D. értekezések

3041.

ANGELI ORSOLYA

Szemészet
című program

Programvezető: Dr. Nagy Zoltán Zsolt, egyetemi tanár

Témavezető: Dr. Schneider Miklós, PhD

DOI:10.14753/SE.2024.3041

OPHTHALMIC APPLICATIONS OF OPTICAL COHERENCE TOMOGRAPHY ANGIOGRAPHY

Assessment of macular vasculature in healthy individuals, in age-related macular degeneration and in ischemic conditions

Ph.D. Thesis

Orsolya Angeli, M.D.

Károly Rácz Clinical Medicine Doctoral School

Semmelweis University

Supervisor:	Miklós Schneider, M.D., Ph.D.
Official reviewers:	Kinga Kránitz, M.D., Ph.D. János Hargitai, M.D., Ph.D.
Head of the Complex Examination Committee:	Judit Fidy, M.D., Ph.D., D.Sc.
Members of the Complex Examination Committee:	Miklós Dénes Resch, M.D., Ph.D. Tibor Milibák, M.D., Ph.D. András Papp, M.D., Ph.D.

Budapest
2024

DOI:10.14753/SE.2024.3041

Table of Contents

List of Abbreviations **5**

1. Introduction **7**

1.1. Historical overview and technical details of optical coherence tomography 7

1.2. Advancements in imaging technology 8

1.3. OCT angiography 8

1.3.1. The potential applications of OCTA in ophthalmology and beyond 10

1.4. Background and review of relevant literature 11

1.4.1. Analysis of retinal vascular density on OCTA images of healthy subjects using two different semi-manual methods 11

1.4.2. Comparison of OCTA, fluorescein angiography, and indocyanine green angiography images in patients with age-related macular degeneration 12

1.4.3. Detecting microvascular and morphological changes in eyes with central retinal non-perfusion 15

2. Objectives **16**

3. Methods **17**

3.1. Analysis of retinal vascular density on OCTA images of healthy subjects using two semi-manual methods 17

3.1.1. Study design and subjects 17

3.1.2. Acquisition and processing of images 17

3.1.3. Method Nr.1. – Mexican hat filtering (MHF) 18

3.1.4. Method Nr.2. – Shanbhag thresholding (ST) 20

3.1.5. Quantitative analysis 21

3.1.6. Quality assessment and statistical analysis 23

3.2. Comparison of OCTA, fluorescein angiography, and indocyanine green angiography images in patients with age-related macular degeneration 25

3.2.1. Subjects 25

3.2.2. Imaging protocol 25

3.2.3. Image registration 26

3.2.4. Measurements 28

3.2.5. Statistics 30

3.3. Detecting microvascular and morphological changes in eyes with central retinal non-perfusion 31

3.3.1. Subjects 31

3.3.2. SS-OCTA 31

3.3.3 SS-OCTA variables 32

DOI:10.14753/SE.2024.3041

3.3.4. SS-OCT variables 33
3.3.5. Statistical analysis 33
4. Results 35
4.1. Analysis of retinal vascular density on OCTA images of healthy subjects using two semi-manual methods 35
4.1.1. ETDRS grid placement, noise reduction, and number of separated vascular segments 35
4.1.2. Comparison of the two methods based on VD, SkD, and VDI parameters 36
4.2. Comparison of OCTA, fluorescein angiography, and indocyanine green angiography images in patients with age-related macular degeneration 42
4.2.1. FAZ area, perimeter, and circularity in FA and SS-OCTA 42
4.2.2. CNV lesion size, perimeter, and circularity in ICGA and SS-OCTA 42
4.3. Detecting microvascular and morphological changes in eyes with central retinal non-perfusion 43
4.3.1. Wide-field fluorescein angiography results 44
4.3.2. Comparison of BRVO and CRVO, NPDR and PDR groups 44
4.3.3. Comparison of DR and RVO groups 44
4.3.4. Descriptive statistics from all patients 46
5. Discussion 47
5.1. Analysis of retinal vascular density on OCTA images of healthy subjects using two semi-manual methods 47
5.2. Comparison of OCTA, fluorescein angiography, and indocyanine green angiography images in patients with age-related macular degeneration 50
5.3. Detecting microvascular and morphological changes in eyes with central retinal non-perfusion 53
6. Conclusions 57
7. Summary 58
8. References 59
9. Bibliography of the candidate's publications 80
9.1. Publications related to the PhD thesis 80
9.2. Publications not related to the PhD thesis 80
10. Acknowledgements 82

DOI:10.14753/SE.2024.3041

List of Abbreviations

AMD	age-related macular degeneration
BCVA	best corrected visual acuity
BRVO	branch retinal vein occlusion
CI	confidence interval
CNV	choroidal neovascularization
CRVO	central retinal vein occlusion
DCP	deep capillary plexus
DR	diabetic retinopathy
DRIL	disorganization of retinal inner layers
ELM	external limiting membrane
ERM	epiretinal membrane
ETDRS	early treatment of diabetic retinopathy study
EZ	ellipsoid zone
FA	fluorescein angiography
FAZ	foveal avascular zone
GCP	Good Clinical Practice
HRF	hyperreflective foci
ICGA	indocyanine green angiography
IRC	intraretinal cysts
LoG	Laplacian of Gaussian
MA	microaneurysm
MAs	microaneurysms
MHF	mexican hat filter
NIH	National Institutes of Health
nAMD	neovascular age-related macular degeneration
OCT	optical coherence tomography
OCTA	optical coherence tomography angiography
OMAG	optical microangiography
PS-OCT	polarization-sensitive optical coherence tomography
RVO	retinal vein occlusion
SCP	superficial capillary plexus

SD	standard deviation
SkD	skeleton density
SD-OCT	spectral-domain optical coherence tomography
SD-OCTA	spectral-domain optical coherence tomography angiography
SS-OCT	swept-source optical coherence tomography
SS-OCTA	swept-source optical coherence tomography angiography
ST	Shanbhag thresholding
TD-OCT	time-domain optical coherence tomography
VAD:	Vascular density
VD	vessel density
VDI	vessel diameter index
VEGF	vascular endothelial growth factor

DOI:10.14753/SE.2024.3041

1. Introduction

1.1. Historical overview and technical details of optical coherence tomography

Optical Coherence Tomography (OCT) is a dynamically evolving imaging technique that is widely used in various fields, including ophthalmology, cardiology, and dermatology.

David Huang, a medical researcher and physician, and James Fujimoto, a physicist and electrical engineer, co-invented OCT in the early 1990s. (2)

During OCT examinations, high-resolution cross-sectional images are created using a special light source. On the images, areas with different optical densities can be distinguished from each other. In vivo, non-invasive, non-contact microscopic-resolution information is obtained, which is why the procedure is also referred to as „optical biopsy". (3)

Due to the extremely high speed of light, the reflections cannot be directly measured. OCT imaging is based on the principle of interferometry, where the light reflected from the examined tissue interferes with a reference beam of light, and the interference pattern is measurable. The imaging that characterizes differences in depth reflectivity, similar to ultrasound terminology, are called A-scans, and the longitudinal OCT images created from multiple A-scans are referred to as B-scans. (4)

The interfaces between structures with different optical properties are displayed according to their optical reflectivity, and they are easily interpreted after grayscale or so-called "false-color" encoding.

The axial resolution of the images is determined by the properties of the light source, while the transverse resolution depends on the optical properties of the eye and the number of acquired A-scans. The depth of the image also depends on the wavelength used, and increasing the wavelength can enhance tissue penetration within certain limits. (4)

1.2. Advancements in imaging technology

Over time, OCT technology improved significantly. Initially using time-domain OCT (TD-OCT), which scanned different depths sequentially, the technology shifted towards spectral-domain OCT (SD-OCT) and swept-source OCT (SS-OCT). SD-OCT and SS-OCT offered faster imaging speeds and improved resolution, enabling better real-time visualization and three-dimensional imaging of tissues. (5)

Functional extensions of OCT have emerged, such as polarization-sensitive OCT (PS-OCT) (6, 7) and Doppler OCT (8, 9), enabling the assessment of tissue properties beyond structural imaging.

Advancements in miniaturization led to the development of handheld OCT devices (10-12), enabling easier access and imaging in various clinical settings. Integration with other imaging modalities and technologies like adaptive optics (13-15) and artificial intelligence (16-19) further enhanced OCT's capabilities and diagnostic accuracy.

1.3. OCT angiography

As a functional extension of existing SD and SS-OCT devices, OCT angiography (OCTA) has become available in the last 5-10 years, rapidly gaining popularity in clinical practice. OCTA is a non-invasive, dye-free imaging procedure, which generates an in vivo cross-sectional image of the ever-changing microvascular network within the choroid and retina (Figure 1). In essence, OCT angiography relies on motion contrast: the machine scans a specific area multiple times and then analyzes the difference between multiple B-scans, which is referred to as decorrelation signal. This method operates on the premise that, in theory, only circulating erythrocytes within the retinal capillaries should exhibit movement within the retina. (20)

Various algorithms have emerged for OCTA techniques, aiming to harness distinct elements within the OCT signal. These methods can be categorized into three groups: (1) OCTA based on phase signals, (2) OCTA based on intensity signals, and (3) OCTA based on complex signals. (21)

DOI:10.14753/SE.2024.3041

Early OCTA systems had limitations like motion artifacts and limited depth penetration. However, advancements in imaging speed, resolution, and software algorithms have addressed these issues, leading to more accurate and detailed imaging. Since OCTA images are highly sensitive to motion artifacts caused by eye movements it is important to note that one of the most defining characteristics of various OCT angiography devices is the quality of their eye tracking system. Eye tracking technology helps compensate for these movements by adjusting the scanning pattern in real-time, resulting in improved image quality and accuracy. Eye tracking enables accurate registration of OCTA images over time or across multiple scans. This is crucial for longitudinal studies, monitoring disease progression, and assessing treatment efficacy.

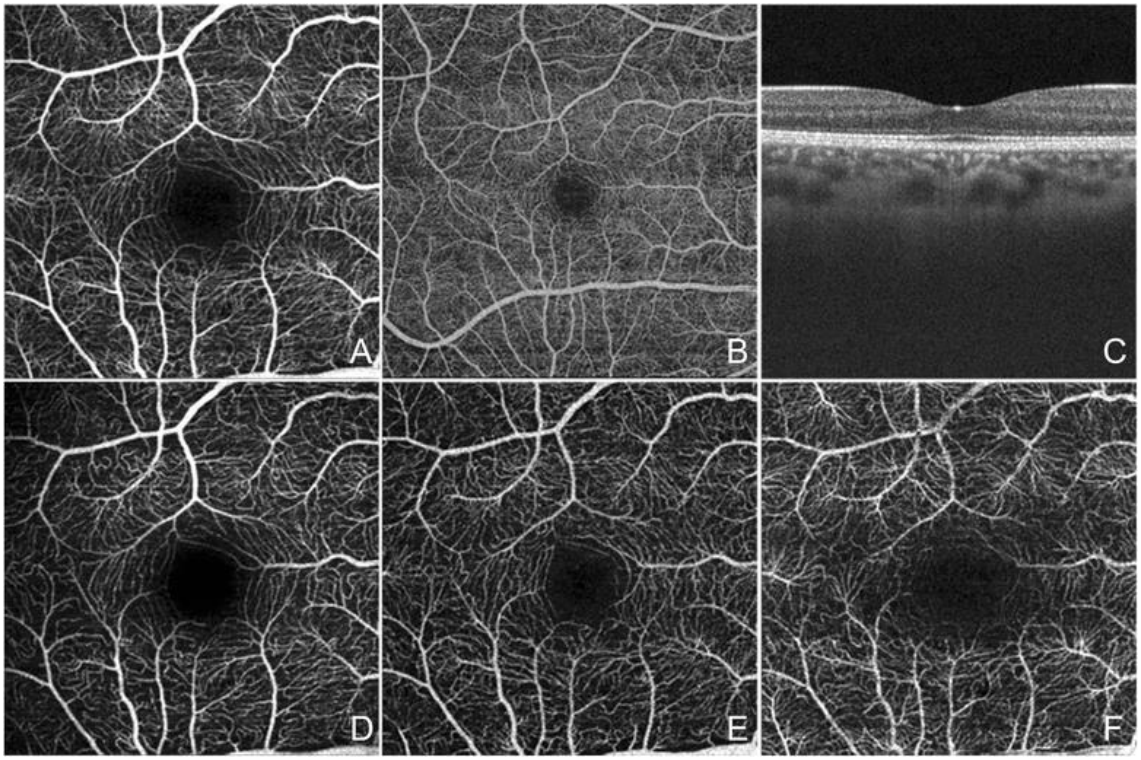

Figure 1. The normal right eye of a 26 year-old Caucasian woman using a prototype swept source optical coherence tomography angiography (OCTA) system (Department of Electrical Engineering and Computer Science and Research Laboratory of Electronics, Massachussetts Insitute of Technology, Cambridge, MA). (**A**) Full-thickness (internal limiting membrane to Bruch's membrane) 3 x 3 mm OCT angiogram. (**B**) Full-thickness 6 x 6 mm OCT angiogram. (**C**) Corresponding OCT b-scan. (**D**) 3 x 3 mm OCT angiogram of the retinal nerve fiber layer plexus of the inner retina. (**E**) 3 x 3 mm OCT angiogram of the ganglion cell layer plexus of the inner retina. (**F**) 3 x 3 mm OCT angiogram of the "deep" inner retina. *Reproduced under CC BY 4.0, from (22)*

1.3.1. The potential applications of OCTA in ophthalmology and beyond

In ophthalmology, OCTA has become instrumental in diagnosing and monitoring various retinal diseases, including diabetic retinopathy (23-25), age-related macular degeneration (AMD) (16, 26, 27), retinal vascular occlusions (28-33), and retinal neovascularization (34-36). It provides detailed images of the retinal vasculature, allowing ophthalmologists to detect abnormalities such as microaneurysms, capillary non-perfusion areas, and neovascularization. OCTA also aids in the evaluation of optic nerve head and peripapillary microvasculature in patients with glaucoma. It can help identify changes in blood flow and capillary density that may be indicative of glaucomatous damage. (37, 38) OCTA provides detailed choroidal imaging, enabling the assessment of choroidal thickness and perfusion in conditions like central serous chorioretinopathy, choroidal neovascularization, and uveitis. (39-42) The technique is also used to study and diagnose vascular abnormalities, such as retinal artery macroaneurysms, retinal arterial and venous tortuosity, and other vascular anomalies. (43, 44)

Ophthalmologists can use OCTA to monitor the effectiveness of treatments, such as anti-VEGF (anti-vascular endothelial growth factor) therapy for AMD and diabetic retinopathy. Changes in retinal and choroidal blood flow can be tracked over time to assess treatment response. (45, 46) It also helps in identifying areas of retinal ischemia, which can be vital in the management of retinal vascular diseases and guiding treatment decisions. (47) OCTA aids in surgical planning for procedures like vitrectomy, allowing surgeons to assess vascular structures and make informed decisions during surgery. (48, 49)

OCTA is a valuable tool for research in ophthalmology and has been used in clinical trials to study the progression of various eye diseases and the effects of experimental treatments. (50)

OCT angiography, originally developed for ophthalmic imaging, has also shown promising potential beyond the field of ophthalmology. OCTA has shown potential in dermatology for imaging cutaneous microvasculature. It aids in assessing skin lesions, evaluating wound healing, and understanding vascular patterns in various skin conditions such as psoriasis, skin tumors, and vascular malformations. (51, 52) In neurology, OCTA

could be used for imaging cerebral blood flow and studying conditions like ischemic stroke, brain tumors, and vascular malformations. (53-55) In neurosurgery, it may aid in preoperative planning by visualizing cerebral vasculature. (56) OCTA holds promise in cardiology for imaging coronary microvasculature. It could assist in assessing coronary artery disease, detecting plaque vulnerability, and studying microvascular diseases affecting the heart. (57) In gastroenterology, OCTA might help visualize microvasculature in the gastrointestinal tract. It could aid in diagnosing and monitoring diseases like inflammatory bowel disease and assessing microvascular changes in tumors. (58) OCTA's capability to image tissue microvasculature is beneficial for assessing engineered tissues' vascularization in regenerative medicine and tissue engineering applications. (59, 60)

1.4. Background and review of relevant literature

1.4.1. Analysis of retinal vascular density on OCTA images of healthy subjects using two different semi-manual methods

Retinal vascular density (VAD) analysis is an important tool in ophthalmology, allowing clinicians to gain deeper insights into the vascular changes occurring in the retina and providing a basis for diagnosis, treatment planning, and monitoring of various retinal diseases. (61-64)

The retina consists of several vascular layers, including the superficial capillary plexus, deep capillary plexus, and choriocapillaris. Each of these layers has a specific role in maintaining retinal function and health. Retinal VAD analysis is used to diagnose and monitor a variety of retinal diseases, including diabetic retinopathy, retinal vascular occlusions, and macular degeneration. Changes in VAD can be indicative of disease progression. It can also be used to assess the impact of glaucoma on retinal blood flow. Reduced vascular density can be a sign of glaucomatous damage. (65) VAD analysis plays a role in certain clinical trials of therapies for retinal conditions. (66, 67)

In recent years, the analysis of retinal VAD using OCTA images has received more attention. Prior to the advent of automated VAD analysis tools like Angioplex Metrix by

Zeiss, AngioAnalytics by Optovue, and Angioscan by Nidek, numerous studies explored the pros and cons of various VAD quantification methods and OCTA devices. (62, 68-70) Moreover, there are alternative software programs, such as MATLAB, ImageJ, and Angiotool, which facilitate semi-manual VAD measurements using binarized and/or skeletonized OCTA images, and these tools are commonly employed in ophthalmological research. (64, 71-73)

The Mexican-hat filter in the ImageJ software is a built-in algorithm that has been used to determine vascular density in numerous scientific publications (63, 74-79) through semi-manual methods. The Shanbhag filter (80), which is also an ImageJ algorithm, has been previously tested for the analysis of retinal vascular density only once. (81)

The semi-manual analysis involves the quantification of parameters such as vessel density (VD, skeleton density (SkD), and vessel diameter index (VDI). These measurements are typically obtained for different retinal layers. (63)

While VAD analysis is a valuable tool, challenges include the need for standardized protocols and algorithms, as measurements can vary between different OCTA devices and software. (82) Additionally, it may be affected by factors like media opacities (e.g., cataracts) and patient cooperation.

1.4.2. Comparison of OCTA, fluorescein angiography, and indocyanine green angiography images in patients with age-related macular degeneration

Optical coherence tomography angiography is becoming more commonly utilized as an initial diagnostic tool in neovascular age-related macular degeneration (nAMD) due to its ability to offer non-invasive, dye-free imaging of retinal and choroidal blood flow, alongside structural information derived from OCT. However, OCTA is not advised as a first-line diagnostic tool in nAMD guidelines, as its sensitivity for detecting choroidal neovascularization (CNV) is lower than the sensitivity of the gold standard fluorescein angiography (FA) (Figure 2 and 3) and indocyanine green angiography (ICGA) (Figure 2 and 3). (83-87)

There are several factors contributing to the variation in detection results between OCTA and FA/ICGA, such as fluid, significant pigment epithelium detachments, hemorrhages, segmentation inaccuracies, as well as the presence of floaters or motion artifacts.

Comparative research has revealed that the foveal avascular zone (FAZ) appears larger in FA images compared to OCTA (88, 89), and the size of CNV lesions is greater in ICGA than in OCTA, resulting in OCTA underestimating the CNV area by approximately 4.5%. (90) In contrast, measurements of corneal neovascularization size exhibit strong agreement between OCTA and ICGA, with OCTA showing a slightly larger lesion size compared to ICGA. (91)

Based on the information provided, it appears that capturing images at the retinal and choroidal levels can be affected by factors such as the recording angle, eye movements, and optical effects. (92) These factors may require correction before making reliable conclusions when comparing areas across different devices and imaging methods. Interestingly, none of the comparative studies have incorporated corrections for potential image distortion, which could introduce bias, particularly in size measurements. (88-90, 93-95)

DOI:10.14753/SE.2024.3041

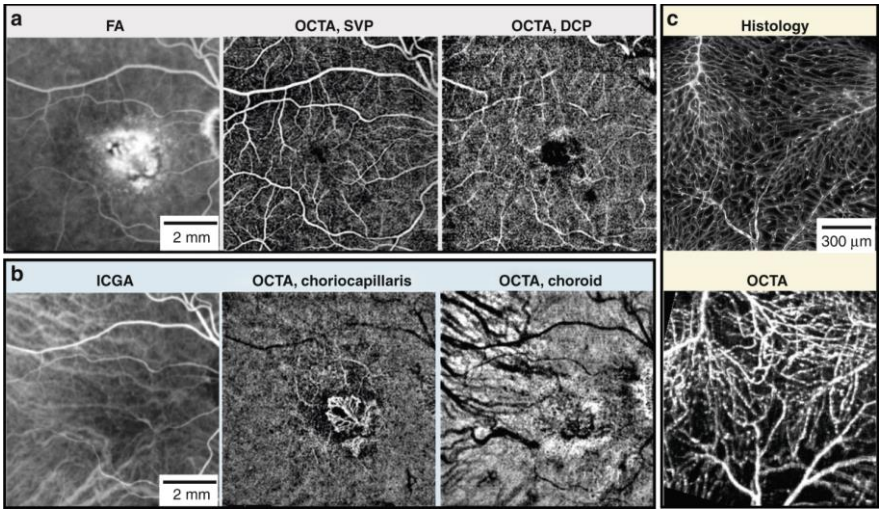

Figure 2. Comparison of OCTA, fluorescein angiography (FA), indocyanine green angiography (ICGA), and histology: **a, b** FA, ICGA, and OCTA segmented to superficial vascular plexus (SVP), deep capillary plexus (DCP), choriocapillaris, and choroid, from a patient with choroidal neovascularization secondary to age-related macular degeneration. a FA shows leakage of dye obscuring details of the fine blood vessels within the choroidal neovascularization that can be more clearly seen in OCTA at the level of choriocapillaris than ICGA in (**b**). **c** Confocal microscopy and OCTA from an isolated perfused porcine eye ex vivo. For the OCTA image acquisition, the whole porcine eyeball was used, and the retinal vasculature was perfused using red blood cells. After the OCTA experiment, retinal vasculature histology was performed. The retina was perfused with fluorescein as a contrast agent, and the eyeball was cut open, flat-mounted and imaged using confocal scanning laser microscopy. Both images are maximum intensity projections from the full retinal thickness. **c** Adapted with permission from Yu et al. (96) *Reproduced under CC BY 4.0, from (97)*

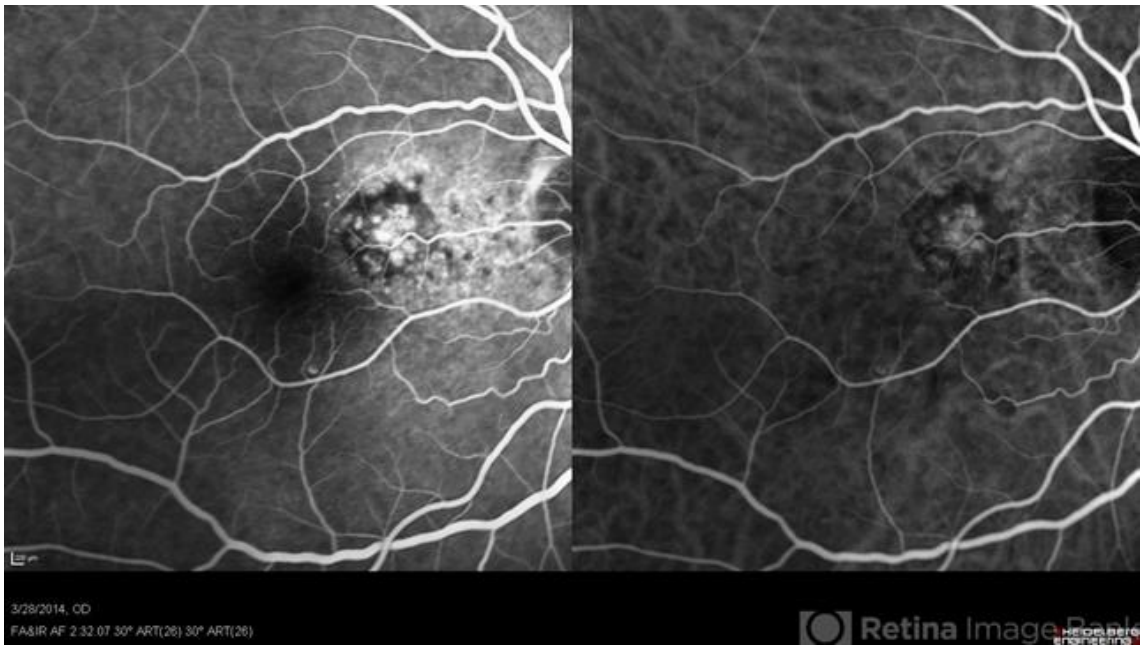

Figure 3. Polypoidal choroidal vasculopathy (PCV): The PCV lesion shows hyperfluorescence and hypercyanescence on intermediate-phase FA (left) and ICGA (right). This image was originally published in the Retina Image Bank® website. Gareth Lema MD, PhD. Photographer Sandra Boglione. Polypoidal Choroidal Vasculopathy - IVFA/ICGA. Retina Image Bank. 2018; 28352. © The American Society of Retina Specialists

DOI:10.14753/SE.2024.3041

1.4.3. Detecting microvascular and morphological changes in eyes with central retinal non-perfusion

Retinal ischemia (98) is a condition characterized by inadequate blood supply to the retina, which can lead to damage or loss of retinal tissue, and consequently to visual impairment or even blindness. Various factors and conditions can contribute to the development of retinal ischemia, including atherosclerosis, hypertension, diabetic retinopathy, retinal artery or vein occlusion, glaucoma, vasculitis, etc., but the most common causes are diabetic retinopathy (DR) and retinal vein occlusion (RVO). (99-103)

In retinal conditions marked by persistent vascular obstructions, it proves challenging to anticipate the onset of ischemia and the resulting functional prognosis.

Several OCT characteristics, including the disruption of the external limiting membrane (ELM), ellipsoid zone (EZ), the presence of hyperreflective foci (HRF), and the disorganization of retinal inner layers (DRIL), have been identified as indicators of retinal ischemia. These features have also been linked to changes in visual acuity. (99) Furthermore, a consistent correlation between the enlargement of the FAZ and a decline in visual function has been observed in numerous studies involving patients with DR and RVO. (100, 101)

In addition to the structural alterations identified in OCT images, certain OCTA parameters, such as vessel density (the area of the segmented vessels in percent), junction density (the frequency of vessel junctions in the image), total vessel length (the sum of Euclidean distances[1] between the pixels of all the vessels in the image), the number of endpoints (the number of open-ended segments), and lacunarity (a variable that indicates spatial dispersion), can offer supplementary insights into the central perfusion status. They also enable the estimation of the degree of central retinal ischemia. (101, 103)

[1] „The Euclidean distance is the ordinary straight line distance between two points in Euclidean space, which can be any nonnegative integer dimension, including the three-dimensional space.” 104. Artin E. Geometric Algebra. Hoboken, NJ, USA: John Wiley & Sons; 2011.

DOI:10.14753/SE.2024.3041

2. Objectives

The aim of our research was to investigate the vascular structure, vascular density, and other structural abnormalities of the retina by processing OCTA images in healthy individuals and in different retinal disorders such as AMD, DR, and RVO.

To achieve these goals, the objectives of the studies presented were as follows:

1. Analysis of retinal vascular density on OCTA images of healthy subjects using two semi-manual methods:

(i). To assess qualitative and quantitative differences in vascular density analysis using both a conventional method (Mexican hat filter) and a novel alternative (Shanbhag thresholding) by determining different vascular parameters

(ii). To compare the two methods based on other factors, such as noise filtering or the number of generated vascular segments during the analysis.

2. Comparison of OCTA, fluorescein angiography, and indocyanine green angiography images in patients with age-related macular degeneration

(i). To make comparisons in area measurements among OCTA, fluorescein angiography, and indocyanine green angiography.

(ii). To utilize deep learning for image registration to correct any potential bias caused by image distortion.

3. Detecting microvascular and morphological changes in eyes with central retinal non-perfusion

(i). To examine OCT and OCTA data in patients with retinal ischemia as a consequence of DM or RVO.

(ii). To explore structural changes related to central retinal non-perfusion and their correlation with visual acuity.

DOI:10.14753/SE.2024.3041

3. Methods

3.1. Analysis of retinal vascular density on OCTA images of healthy subjects using two semi-manual methods

3.1.1. Study design and subjects

This observational study was conducted at Semmelweis University's Department of Ophthalmology in Budapest, Hungary. The research adhered to ethical guidelines outlined in the Declaration of Helsinki. The study protocol received approval from the National Institute of Pharmacy and Nutrition in Hungary under Approval Number OGYÉI/1253/2017 and was registered prospectively on ClinicalTrials.gov (Identifier: NCT03590899). Patients were comprehensively informed about the examinations and provided written consent.

A total of 38 eyes from 38 healthy volunteers aged between 24 and 83 years (17 males and 21 females), were included in this investigation. Exclusion criteria included any current or past retinal diseases or glaucoma, prior ocular surgeries, or laser photocoagulation, as well as any optical media opacities that could potentially affect the quality of captured images.

3.1.2. Acquisition and processing of images

The subjects in this study were scanned using the Zeiss Cirrus HD-OCT 5000 AngioPlex SD-OCT device (Carl Zeiss Meditec Inc. in Dublin, CA, USA). This device operates at a speed of 68,000 A-scans per second, utilizing an 840-nm superluminescent diode with a bandwidth of 45 nm. To visualize the microvasculature, the device employs the optical microangiography (OMAG) segmentation algorithm, which considers both amplitude and phase aspects of the entire OCT signal. Additionally, it is equipped with a FastTrac™ eye tracker to minimize the impact of involuntary eye movements.

The AngioPlex system has the capability to separately visualize vessels in the superficial retina, the deep retinal layer, the choriocapillaris, and other large choroidal vessels, similar to other OCTA systems. A 6×6 mm square area, centered on the fovea,

was scanned in both eyes of all study subjects. The vascular plexuses were segmented using the device's built-in software. To ensure the quality of the images, two investigators (O.A. and M.S.) individually inspected them for proper centering, absence of artifacts, and correct segmentation. Any discrepancies were resolved through discussion. We only included those images in the study where the signal strength measurement indicated by the Zeiss Angioplex software was at least 8/10. The right eye of each patient was included in the analysis, and in cases where the image quality was suboptimal, scans of the left eye were used. Subsequent to image acquisition, two different post-processing methods, Mexican hat filtering (MHF) and Shanbhag thresholding (ST), were applied to each image of the superficial vascular plexus. Three distinct parameters were assessed: Vessel Density (VD), Skeleton Density (SkD), and Vessel Diameter Index (VDI).

3.1.3. Method Nr.1. – Mexican hat filtering (MHF)

ImageJ is an open-source image processing and analysis software developed by the National Institutes of Health (NIH) in the United States. It is widely used for a variety of tasks related to image analysis. (105) In ImageJ, the "Mexican Hat" filter refers to a type of image filter used for image processing and analysis. It is also known as the Laplacian of Gaussian (LoG) filter or the second derivative of a Gaussian filter. This filter is designed to enhance or detect edges and fine details in an image while suppressing noise. (1) The methodology for this image processing technique has been extensively described by Kim et al. (63)

To begin, OCTA images were imported from the OCT device into the digital image processing software GIMP (version 10.4, The GIMP Team, Charlotte, NC, USA), where they were subsequently converted into 16-bit tiff files. Further manipulations were carried out using ImageJ (version 1.52a), with the following steps.

First, image filtering was applied. Noise reduction was achieved by employing a minimum filter with a 2×2 pixel size.

In the second step, FAZ was manually eliminated. In ImageJ, we employed the "freehand selection" tool to outline the area of interest and subsequently utilized the "cut" function to remove the selected region.

DOI:10.14753/SE.2024.3041

Subsequently, the next step involved binarizing the sample. To achieve this, we applied the MHF to obtain representative expansion data with binarized values. Finally, we utilized the built-in skeletonization function in ImageJ to extract length-type information from the processed image (Figure 4).

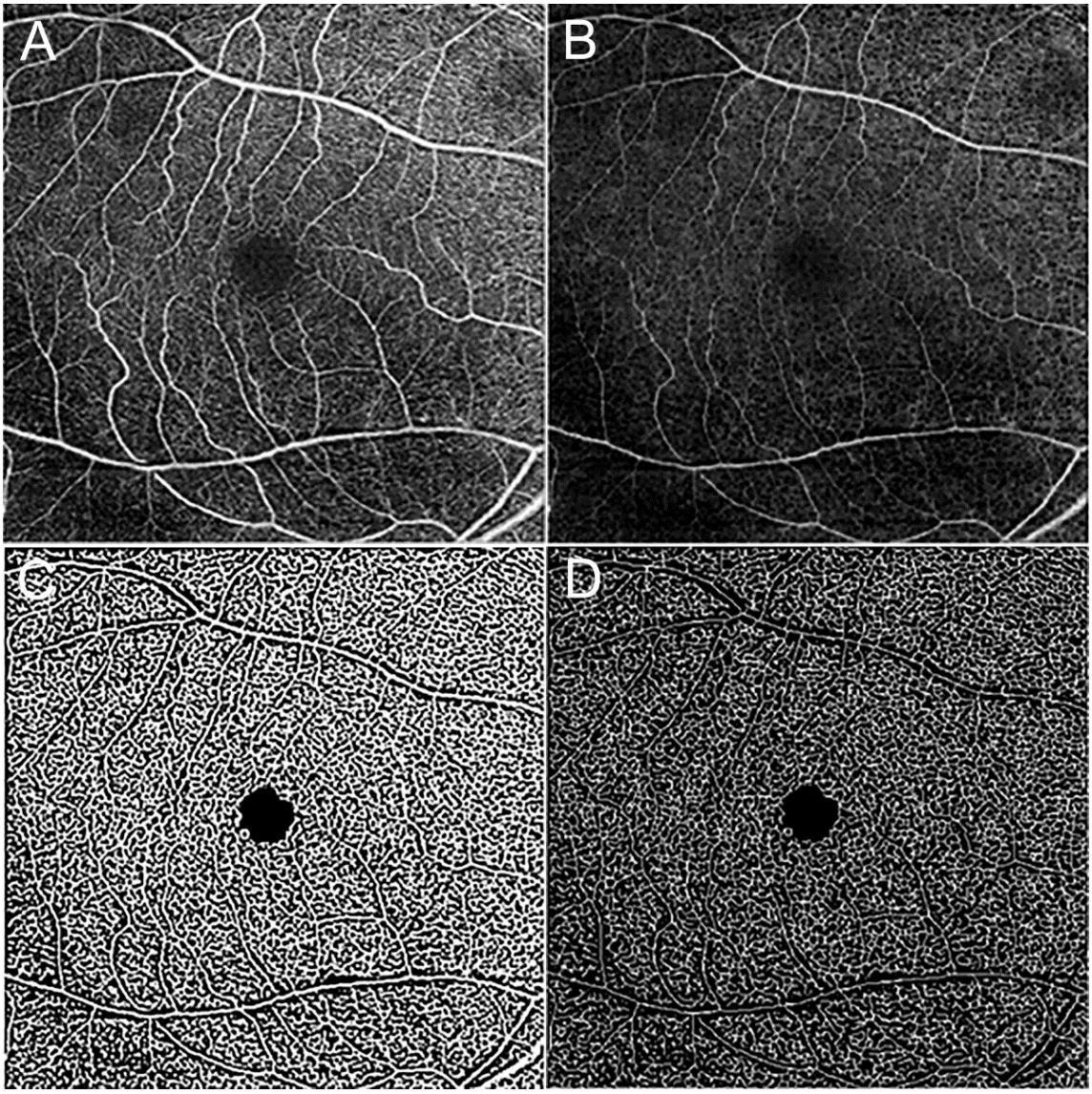

Figure 4. The steps of image processing with Mexican hat filtering method: **(A)** Original image, **(B)** Minimum filtered image with removed avascular zone, **(**C**)** Mexican hat filtered image, **(**D**)** Skeletonized image.

Reproduced under CC BY 4.0, from (1)

3.1.4. Method Nr.2. – Shanbhag thresholding (ST)

Shanbhag thresholding is a method used in image processing to automatically segment or threshold an image into two distinct regions: foreground and background. This technique is designed to find an optimal threshold value that separates objects of interest from the background in a way that minimizes information loss and maximizes image quality. (1)

In ImageJ, Shanbhag thresholding is one of the built-in thresholding methods. It is based on the work of Arvind Shanbhag (80) and calculates the threshold by considering the statistical properties of pixel intensities in the image. The algorithm takes both the mean and variance of pixel intensities within the two regions into account to determine an optimal threshold value. This helps to ensure that the resulting binary image retains as much relevant detail as possible while minimizing the impact of noise. (1)

During our image processing, the initial two steps mirrored those of the MHF method, which involved importing the image and converting it to 16-bit, followed by applying a minimum filter. Following these steps, we proceeded with the Shanbhag thresholding process.

Manual removal of the FAZ was not necessary, as this step is automated by ST. In the last step, we conducted image skeletonization (Figure 5).

DOI:10.14753/SE.2024.3041

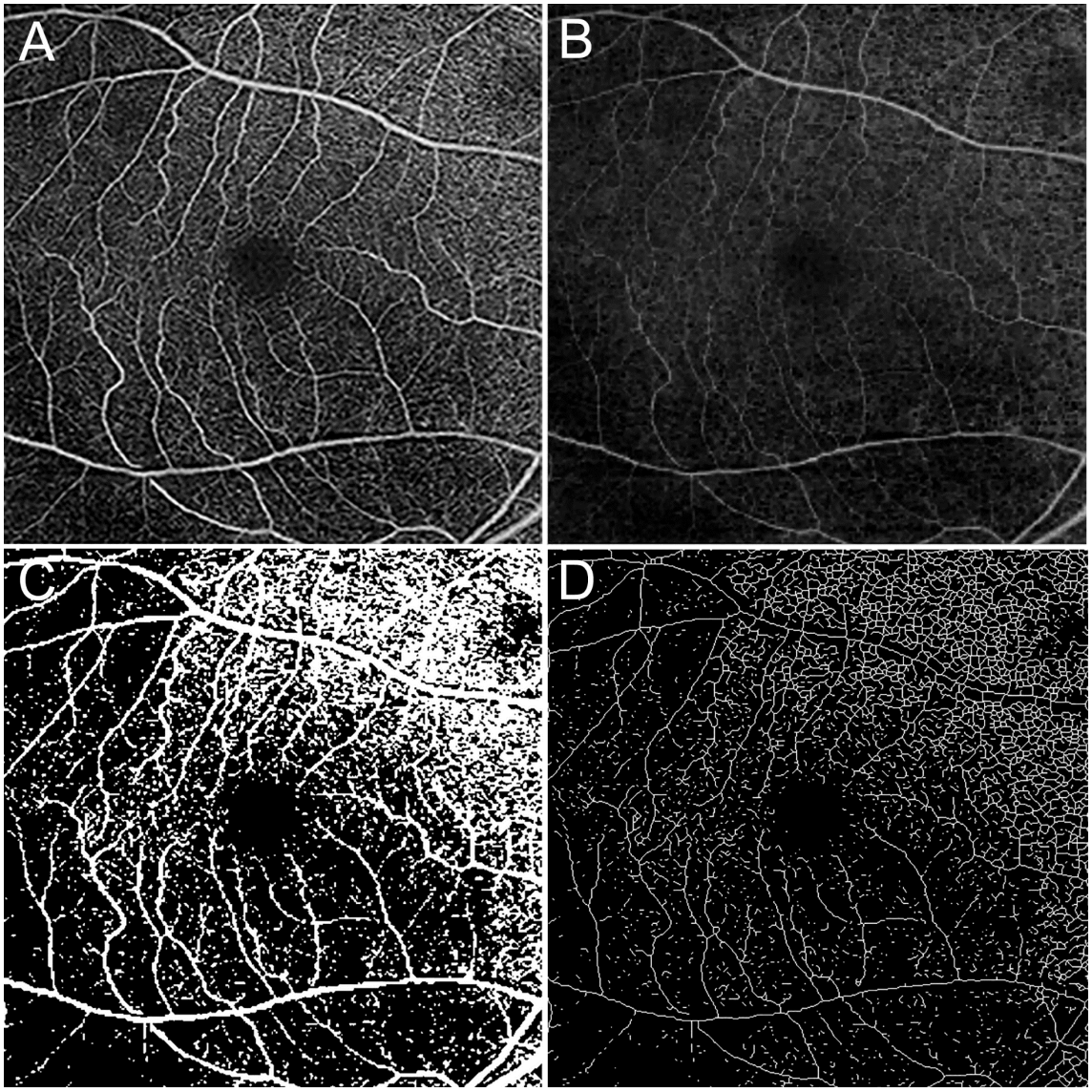

Figure 5. The steps of image processing with Shanbhag thresholding method: **(A**) Original image, **(B)** Minimum filtered image, (**C**) Shanbhag thresholded image with automatically removed avascular zone, (**D**) Skeletonized image. *Reproduced under CC BY 4.0, from* (1)

3.1.5. Quantitative analysis

Quantitative analysis was performed on post-processed images generated by both methods. Vessel density (VD), Skeleton density (SkD), and Vessel diameter index (VDI) were assessed across all nine sectors (Figure 6) defined by the Early Treatment Diabetic Retinopathy Study (ETDRS). (106)

VD serves as a measure of the blood vessel surface. It is determined as a dimensionless ratio, representing the portion of the total image area occupied by the

identified OCTA signal (binarized as white pixels) relative to the entire retinal area (total number of pixels) depicted on the binarized image. (1, 63)

$$\mathrm{VD} = \frac{(\text{white pixels})^2}{(\text{total number of pixels})^2}$$

SkD is calculated by assessing the proportion of the image area occupied by the skeletonized representation of blood vessels. The skeletonization process reduces the vessels to their essential centerlines or skeleton, allowing for a focused analysis of the vascular network's density. This density measurement represents the skeletal structure's coverage within the total image area (mm/mm2). The calculation involves considering the pixels forming the skeletonized vessels in relation to the entire retinal image area. (1, 63)

$$\mathrm{SkD} = \frac{(\text{white skeletonized pixels})}{(\text{total number of pixels})^2}$$

VDI provides information about the actual blood supply to the retina. The calculation involves using both the binary blood vessel image and the skeletonized image. It aims to determine the average vessel volume in the spectral-domain OCTA (SD-OCTA) image, measured in pixels. It is calculated as a ratio of VD and SkD. (1, 63)

$$\mathrm{VDI} = \frac{(\text{white pixels})^2}{(\text{white skeletonized pixels})} = \frac{\mathrm{VD}}{\mathrm{SD}}$$

DOI:10.14753/SE.2024.3041

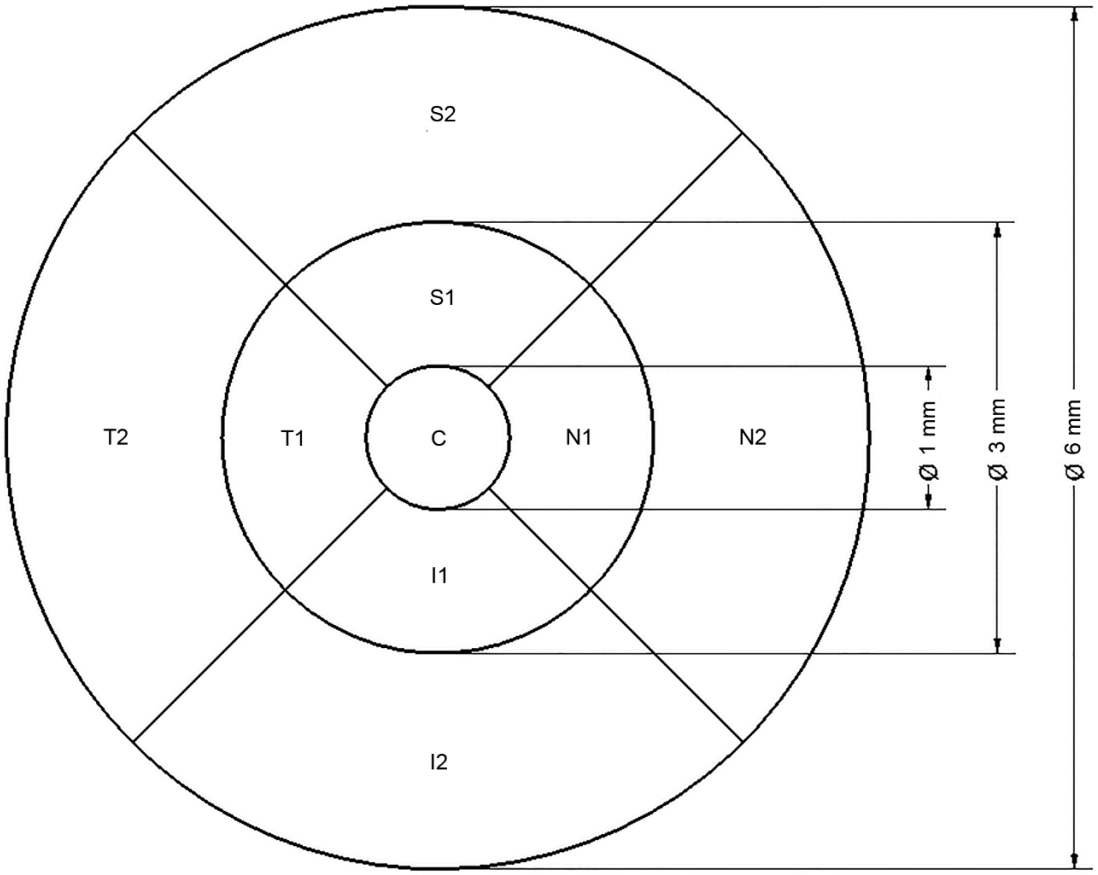

Figure 6. The nine sectors based on the Early Treatment Diabetic Retinopathy Study (ETDRS). Circles are centered around the fovea with diameters of 1, 3 and 6 mm, respectively. Indexes in the sectors refer to their locations as follows: S = superior, N = nasal, I = inferior, T = temporal. Sectors marked with '1' (S1, N1, I1 and T1) are in the inner circle, sectors marked with '2' (S2, N2, I2 and T2) are in the outer circle. Sector 'C' represents the central area. This figure illustrates a right eye. The sector numbers in the text correspond to the grid sectors on this illustration as follows: 1 = C, 2 = I1, 3 = T1, 4 = S1, 5 = N1, 6 = I2, 7 = T2, 8 = S2, 9 = N2.

Reproduced under CC BY 4.0, from (1)

3.1.6. Quality assessment and statistical analysis

After completing image acquisition, post-processing, and data collection, a statistical analysis was conducted. Given the manual placement of the ETDRS grid on each image to ensure proper alignment with the FAZ, an error calculation was performed. As

mentioned earlier, the MHF method required a freehand selection to delineate FAZ boundaries, introducing the possibility of errors in the inner sectors. Error calculation involved manually selecting the FAZ five times and determining the average differences in white pixel count compared to all the white pixels in the zone. In contrast, with ST, this error calculation was unnecessary as the technique automatically marked out the FAZ area.

We conducted a comparison of the two methods, considering both the noise level and the quantity of separated vascular segments.

In the absence of vascular disorders, blood vessels form a single, continuous segment. However, due to the diverse filters and image-processing methods applied, different noise artifacts may manifest in the image, leading to potential fragmentation of the vascular network into distinct segments. As noise increases, the sample quality diminishes, and the vascular network becomes more fragmented. MATLAB (version R2017B, The MathWorks, Natick, Massachusetts, USA) was employed to count the number of segments in each processed image, and these counts were averaged across all processed images for each method.

The verification of differences in values measured by the two methods was carried out graphically in every case. The results of these checks revealed, that the differences in measurements were normally distributed for every parameter in all sectors. For all measured parameters, mean and standard deviation values were computed in each sector, and their distributions were compared using box plots. The agreement between the two processing methods was assessed through Bland–Altman plots (107) for all parameters and sectors. In each instance, the difference between measurements was calculated by subtracting the value of the ST parameter from the value of the MHF parameter. Alongside the mean difference, the limits of agreement (± 1.96*SD) were determined. The assumption of normality for the difference scores was visually checked in each case. The statistical significance of the mean difference was analyzed using the 95% confidence interval.

Statistical calculations were executed with the R system (R Core Team, Vienna, Austria, software version 4.0.4) (108), utilizing the following packages: data.table (109), BlandAltmanLeh (110), ggplot2 (111), and ggpubr (112).

3.2. Comparison of OCTA, fluorescein angiography, and indocyanine green angiography images in patients with age-related macular degeneration

3.2.1. Subjects

This prospective case series study included a consecutive series of 24 treatment-naïve patients with neovascular age-related macular degeneration (nAMD) who presented at the Department of Ophthalmology of the Medical University of Vienna, Vienna, Austria. All participants signed informed consent to participate in the study. The study protocol received approval from the Ethics Committee of the Medical University of Vienna, Vienna, Austria. The study was carried out in accordance with the Declaration of Helsinki, including its latest revisions and adhered to the guidelines of Good Clinical Practice (GCP). The inclusion criteria included individuals aged 50 years or older with a diagnosis of treatment-naïve Type 1 or Type 2 nAMD, and clear ocular media.

Exclusion criteria included any preexisting treatment or other eye disease. Additionally, individuals with a refractive error exceeding ±6 diopters (spherical equivalent) or those with an allergy to intravenous dye (fluorescein or indocyanine green) injection were not included in the study.

3.2.2. Imaging protocol

During the same visit, all patients underwent best-corrected visual acuity testing using Snellen charts, a comprehensive ophthalmic examination that included biomicroscopy and funduscopy, as well as SD-OCT and fluorescein angiography (FA) using the Spectralis HRA + OCT system (Heidelberg Engineering, Heidelberg, Germany), for the diagnosis of nAMD. Following best-corrected visual acuity assessment, the pupil of the study eye was dilated for the SD-OCT and FA examinations. We assessed the peripheral ischemia of patients using wide-field fluorescein angiographies to create two comparable cohorts with similar peripheral nonperfusion status. The wide-field angiography (120˚) for RVO patients was analyzed using the Heidelberg Spectralis (Heidelberg Engineering, Heidelberg, Germany). For DR patients, ultrawide field (200˚) angiographies were

routinely performed using the Optos California (Optos, Optomap, North America). To make these images comparable, we evaluated only the same field of view (approximately 120˚) from the Optomap images. Three groups were established to quantify peripheral ischemia based on the extent of nonperfusion: no ischemia, ≤ 5 disc diameters, or > 5 disc diameters of peripheral ischemia. Additionally, indocyanine green angiography (ICGA) using the Spectralis HRA + OCT system and swept-source optical coherence tomography angiography (SS-OCTA) images were acquired with the PLEX Elite 9000 by Carl Zeiss Meditec, Dublin, CA.

A volumetric flow scan measuring 6x6 mm and consisting of 500x500 A-scans was captured utilizing a 1,060-nm SS-OCTA device. The device operated at an A-scan rate of 100,000 with an axial resolution of 6.3 μm.

The automated layer segmentation shows a predefined vascular plexus, encompassing, among others, the superficial and deep retinal capillary plexus, outer retina to choriocapillaris, and the choroidal capillary layer in orthogonal view. If necessary, manual correction of the automated layer segmentation was performed using the corresponding structural B-scans.

Images were required to include the entire lesion area and were discarded if the signal-to-noise ratio was less than 6 out of 10, if there were motion artifacts, or if floaters were present in the area of interest.

3.2.3. Image registration

Fluorescein angiography, indocyanine green angiography, and SS-OCTA images were exported as Windows bitmap (bmp) files and registered using a deep-learning approach. The vessel appearance served as the basis for FA and ICGA images with the superficial plexus of SS-OCTA images. The algorithm employed is grounded in UNet, a deep-learning algorithm designed for the segmentation of biomedical images. (113) This algorithm effectively segments blood vessels in FA, ICGA, and SS-OCTA images. A model based on UNet and Mask R-CNN was trained for each imaging modality. (114)
The registration process involves a two-step approach. In the initial step, vessel junctions are utilized to estimate scaling, translation, and rotation. In the second step, automated fine-tuning is implemented using vessels, the original images, and the elastix framework.

(115) Ultimately, the registration matrix is applied to the FA and ICGA images (Figure 7). The Elastix Image Registration Toolbox is an open-source software package for medical image registration. It provides a framework for various types of image registration tasks, including rigid, affine, and deformable transformations. Elastix is widely used in the medical imaging community for tasks such as aligning images from different modalities (e.g., CT and MRI), tracking changes in images over time, and integrating information from multiple imaging sources. The registration matrix represents the transformation that needs to be applied to one image to bring it into alignment with another. Depending on the type of transformation being used (e.g., rigid, affine, deformable), the registration matrix can take different forms. In image registration, the goal is typically to find the parameters of the registration matrix that minimize the difference between the images being aligned. This optimization process is often done using optimization algorithms such as gradient descent or Gauss-Newton methods. (116)

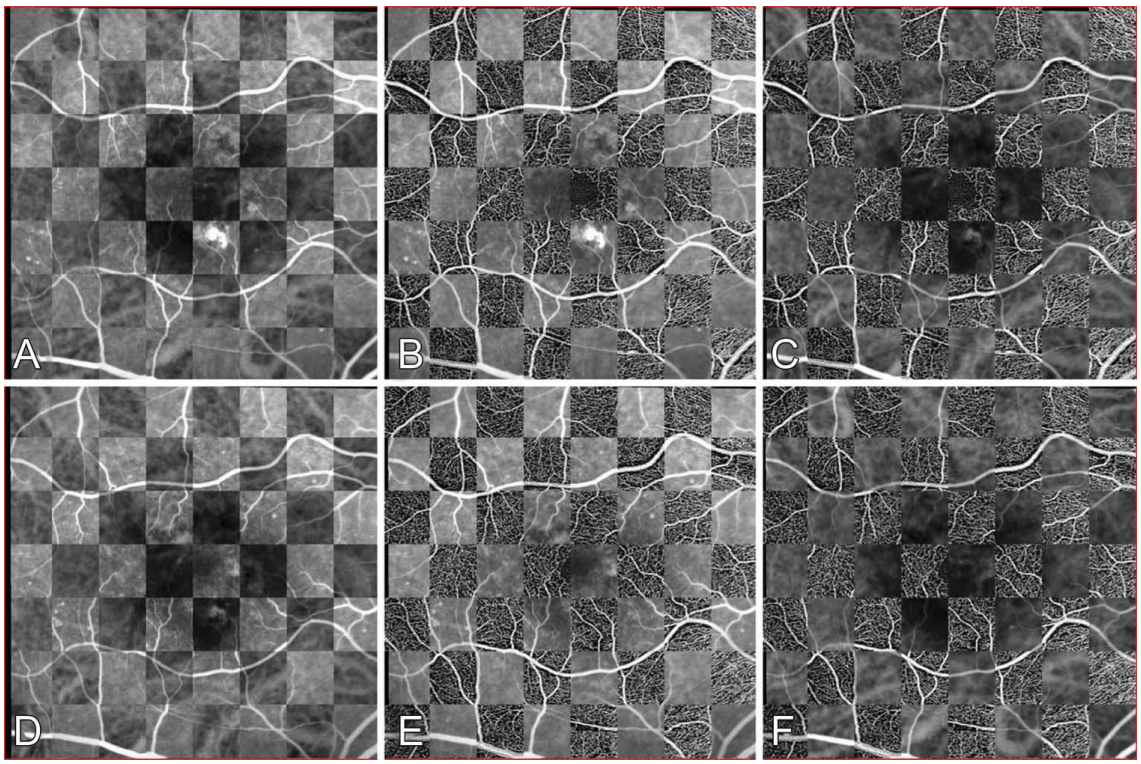

Figure 7. Visual feedback for the registration process of FA/ICGA images with the superficial SSOCTA slab; checkerboard feedback: (**A**) FA-ICGA, (**B**) FA-SSOCTA, (**C**) ICGASSOCTA, (**D**) ICGA-FA, (**E**) SSOCTA-FA, and (**F**) SSOCTA-ICGA.
Reproduced with the publisher's permission, from (16)

DOI:10.14753/SE.2024.3041

3.2.4. Measurements

A single grader analyzed the registered FA, ICGA, and OCTA images using Fiji 1.50e software (Image J, National Institutes of Health). (117)

The freehand tool was employed to outline the FAZ area on the superficial retinal capillary plexus in both fluorescein angiography and swept-source optical coherence tomography angiography (Figure 8). Similarly, the tool was used to delineate the choroidal neovascularization (CNV) lesion size on both ICGA and SS-OCTA outer retina to choriocapillaris or retinal pigment epithelium (RPE)–RPE fit slabs (Figure 9).

The hyper-cyanescent core lesion in ICGA images was chosen by identifying vascular networks at the location of the CNV complex, excluding areas of subsequent dye leakage. The FAZ and CNV lesion area, perimeter, and circularity were then exported for further analysis. The FAZ/CNV lesion area was defined as the size of the segmented FAZ/CNV region, and the perimeter was determined by the length of the FAZ/CNV contour. The circularity was "calculated as an index using the formula where circularity = $4\pi(\text{area}/\text{perimeter}^2)$, indicating the compactness of shape relative to a circle". (118) A circularity value of 1.0 indicates a perfect circle, while a reduced value indicates an increasingly elongated polygon. (16)

DOI:10.14753/SE.2024.3041

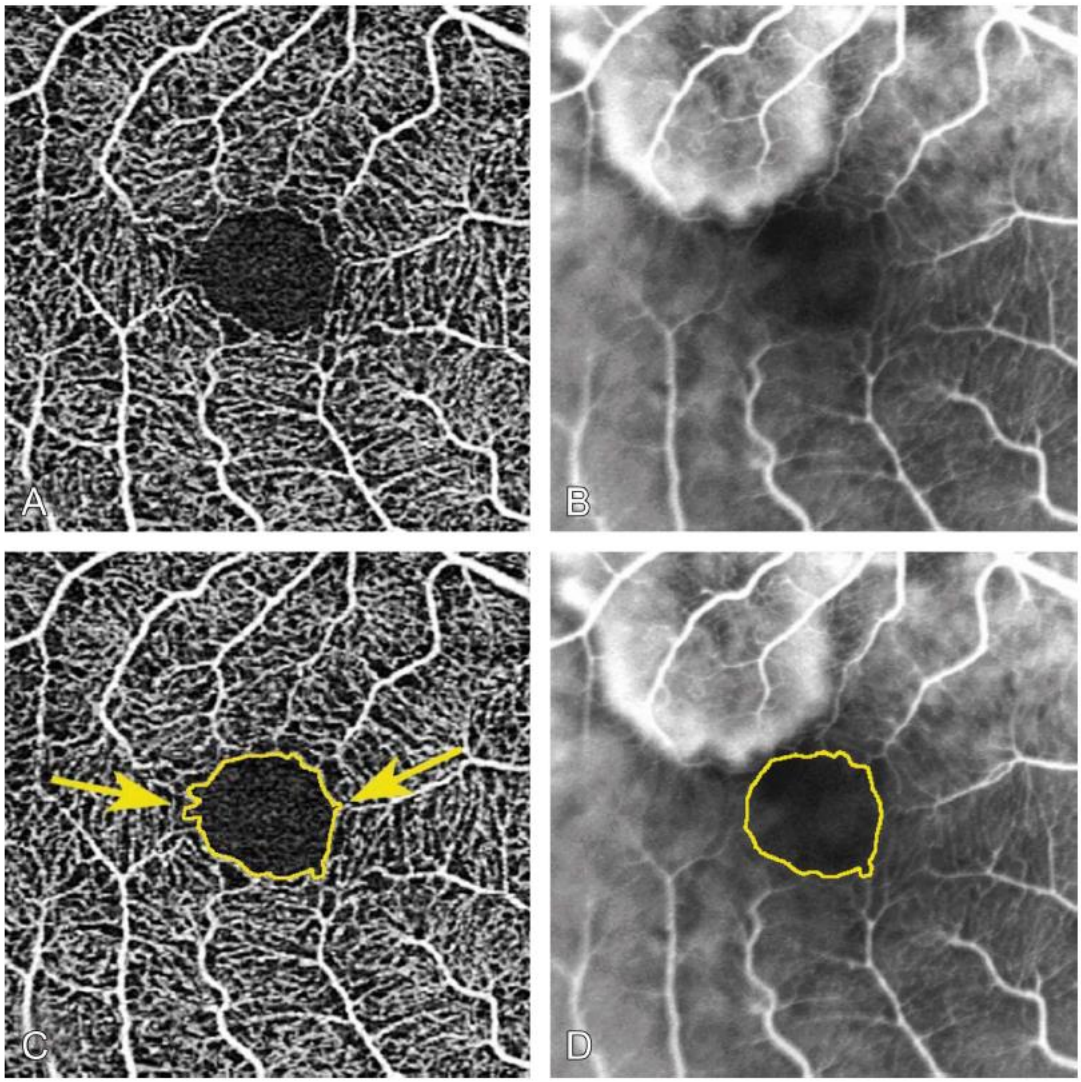

Figure 8. Cropped superficial SSOCTA slab to better visualize the FAZ; (B) cropped FA image to better visualize the FAZ; (C) Cropped superficial SSOCTA slab with delineated FAZ area (yellow line). Yellow arrows indicate areas of different FAZ delineations between SSOCTA and FA; and (D) Cropped FA image with delineated FAZ in yellow.

Reproduced with the publisher's permission, from (16)

DOI:10.14753/SE.2024.3041

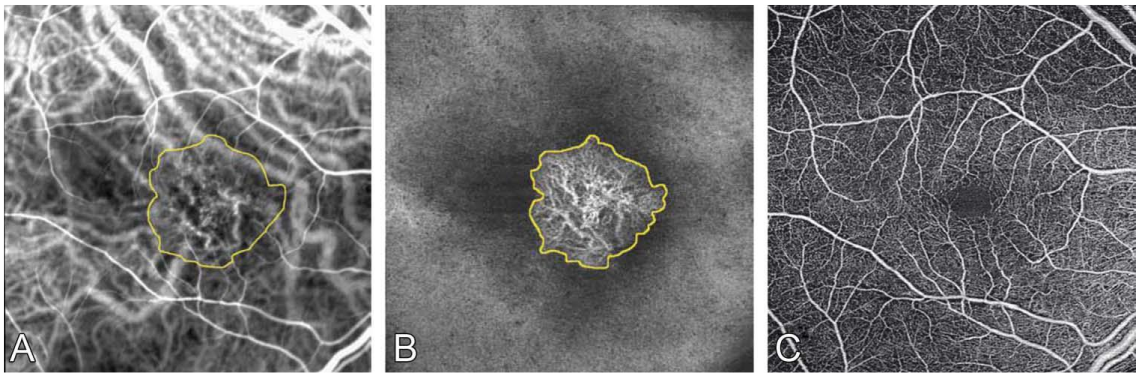

Figure 9. A. Registered ICGA image with CNV delineation in yellow; (**B**) SSOCTA RPE–RPE fit slab with CNV delineation in yellow; and (**C**) the SSOCTA superficial slab which was used for image registration with the ICGA image in (**A**).
Reproduced with the publisher's permission, from (16)

3.2.5. Statistics

Statistical analysis was performed using Prism 6 (SoftPad Software Inc, La Jolla, CA). The D'Agostino-Pearson test was applied to test data for normal distribution. Comparative analyses between FA/ICG and SS-OCTA measurements utilized the Student t-test, Pearson correlation, and Bland–Altman method. Bland–Altman analysis was employed to evaluate agreement between delineations, providing the bias (mean difference) with a predefined limit of agreement of ±1.96 standard deviations, equivalent to the 95% confidence interval (CI). The significance level was set at $P = 0.05$.

3.3. Detecting microvascular and morphological changes in eyes with central retinal non-perfusion

3.3.1. Subjects

For this retrospective cross-sectional study, data from the Department of Ophthalmology and Optometry at the Medical University of Vienna, Austria, from October 2016 to June 2019, were included.

This study was conducted in accordance with the Declaration of Helsinki, including its latest revisions and adhered to the guidelines of Good Clinical Practice (GCP). The study protocol received approval from the Ethics Committee of the Medical University of Vienna.

Forty-four eyes of 44 patients (22 with RVO, 22 with DR) were analyzed. The mean age was 60.55± 11.38 years and mean BCVA was 0.86 ± 0.36 (Snellen, 6m). The affected eye of RVO patients and a random eye of the diabetic patients was selected.

The inclusion criteria for this study comprised the following: (1) presence of center-involving retinal ischemia on OCTA, (2) diagnosis of either diabetic retinopathy (DR) or retinal vein occlusion (RVO), (3) absence of clinically significant macular edema, (4) clear ocular media and high image quality, (5) absence of other concurrent ocular diseases. Exclusion criteria were intravitreal anti-VEGF treatment within 8 weeks prior to potential study inclusion, central laser treatment, and patients who had undergone intravitreal steroid injections, received intravitreal steroid implants, or underwent central laser treatment were not included in the study.

Retinal ischemia was assessed initially through a subjective evaluation of OCTA images. Those images showing nonperfusion in a minimum of one-third of the entire 6x6mm image were categorized as having center-involving ischemia and were consequently included in the analysis.

3.3.2. SS-OCTA

Examinations of all patients took place after pupil dilatation, with the Topcon DRI-OCT Triton swept-source OCT/-A from Topcon, Japan. This SS-OCTA device utilizes a

1050-nm swept-source with an A-scan rate of 100,000 scans per second. Operating with the OCTARA (OCTA ratio analysis) algorithm, the SS-OCTA device enhances the detection sensitivity of low blood flow and minimizes motion artifacts, while maintaining axial resolution. (119)

For each eye, a 6x6-mm volumetric flow-scan, centered on the fovea, was recorded. The automated layer segmentation revealed the predetermined vascular plexuses, including the superficial and deep retinal capillary plexus, the outer retina to choriocapillaris, and the choroidal capillary layer in orthogonal view. Manual corrections were applied to the layer segmentation whenever deemed necessary.

3.3.3 SS-OCTA variables

The variables extracted from SS-OCTA images included the FAZ and vascular parameters. The FAZ was manually delineated by the same investigator on the superficial capillary plexus slab of the 6x6 mm SS-OCTA scans (Figure 10) using the free-hand tool in ImageJ (National Institute of Health, Bethesda, MD, USA).

SS-OCTA images of the superficial capillary plexus (SCP) underwent additional analysis using a semi-automated vessel analyzing software, AngioTool 64 (Version 0.6a). (71)

This program segments and skeletonizes blood vessels, enabling the calculation of morphometrical measurements for the vessels.

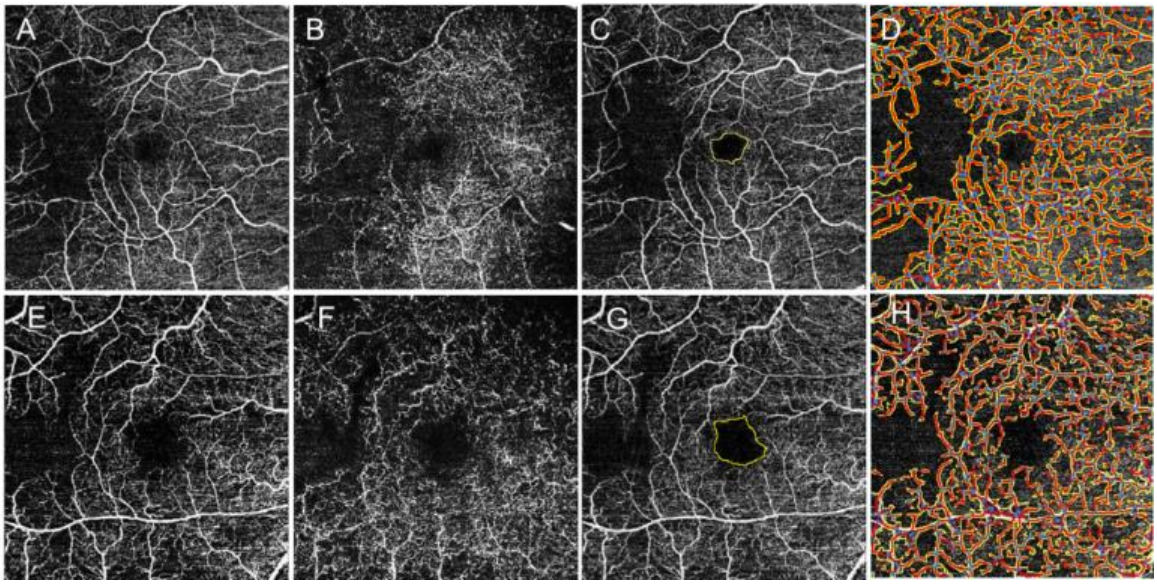

Figure 10. OCTA images of patients with pronounced ischemia. A 52-year-old patient with severe DR above (**A-D**), a 57-years-old male patient with CRVO below (**E-H**). (**A**) superficial capillary plexus of the diabetic patient; (**B**) deep capillary plexus of the diabetic patient; (**C**) yellow line indicates the FAZ area of the diabetic patient; (**D**) AngioTool analysis of the superficial plexus of the diabetic patient; (**E**) superficial capillary plexus of the RVO patient; (**F**) deep capillary plexus of the RVO patient; (**G**) yellow line indicates the FAZ area of the RVO patient; and (**H**) AngioTool analysis of the superficial plexus of the RVO patient. *Reproduced under CC BY 4.0, from (28)*

3.3.4. SS-OCT variables

For each eye, seven OCT scans were evaluated by the same investigator, including one central B-scan and three B-scans both above and below the foveal scan. This approach aligns with the methodology outlined in a previous study by Sun et al. (120) Various features such as intraretinal cysts (IRC), microaneurysm (MA), hyperreflective foci (HRF), epiretinal membrane (ERM), ellipsoid zone (EZ) and external limiting membrane (ELM) disruption, and disorganization of retinal inner layers (DRIL) were documented.

3.3.5. Statistical analysis

The statistical analysis was conducted using SPSS V23 (IBM, Corp., Armonk, N.Y., USA).

Initially, the subgroups of retinal vein occlusion (RVO) were compared, distinguishing between central retinal vein occlusion (CRVO) and branch retinal vein

occlusion (BRVO), and diabetic retinopathy (DR), distinguishing between non-proliferative diabetic retinopathy (NPDR) and proliferative diabetic retinopathy (PDR). This comparison aimed to assess whether there were any differences in the distribution of the parameters among these subgroups.

For the subsequent statistical analysis, we pooled the subgroups into a unified RVO group and a DR group. Comparisons of SS-OCT and SS-OCTA variables between DR and RVO eyes were carried out using ANOVA for parametric measures and the Mann-Whitney U-Test for non-parametric measures. Dichotomous variables underwent comparison using the Chi-square test. Correlations between the parameters were computed using the Spearman test, and correlations between dichotomous variables were assessed through Point Biserial Correlation analysis. A p-value of < 0.05 was considered significant, and Bonferroni correction was implemented to address multiple testing.

4. Results

4.1. Analysis of retinal vascular density on OCTA images of healthy subjects using two semi-manual methods

4.1.1. ETDRS grid placement, noise reduction, and number of separated vascular segments

Errors in determining the ETDRS sectors manually resulted in a low overall error rate of 0.58%. Using the MHF technique, the average errors in the FAZ and inner sectors caused by the freehand selection were 3.5% and 0.5%, respectively.

Regarding noise reduction, both methods were nearly indistinguishable. The noise levels measured with the MHF and the ST were 65.8% and 65.24%, respectively. For each processed image, we counted and averaged the number of separated vascular segments. Using the MHF, we observed a 40% higher fragmentation in the vascular network compared to the ST method (mean 3999 ± 469 versus 2390 ± 361 separated segments with MHF and ST, respectively). Tables 1 and 2 provide detailed breakdowns of VD, SkD, and VDI parameters computed by both MHF and ST across all ETDRS sectors.

Table 1. Parameters calculated by Mexican hat filtering. ETDRS Early treatment of diabetic retinopathy study, *SkD* skeleton density, *VD* vessel density, *VDI* vessel diameter index, *SD* standard deviation. *Reproduced under CC BY 4.0, from (1)*

	ETDRS Sectors								
	1	**2**	**3**	**4**	**5**	**6**	**7**	**8**	**9**
SkD Mean (SD)	0.054 (0.038)	0.119 (0.017)	0.12 (0.014)	0.12 (0.013)	0.118 (0.015)	0.124 (0.012)	0.134 (0.01)	0.123 (0.011)	0.117 (0.011)
VD Mean (SD)	0.134 (0.095)	0.31 (0.045)	0.308 (0.038)	0.313 (0.034)	0.304 (0.043)	0.334 (0.033)	0.362 (0.028)	0.332 (0.028)	0.304 (0.029)
VDI Mean (SD)	2.459 (0.144)	2.603 (0.089)	2.567 (0.064)	2.606 (0.062)	2.568 (0.069)	2.702 (0.092)	2.71 (0.084)	2.693 (0.079)	2.613 (0.064)

Table 2. Parameters calculated by Shanbhag thresholding. ETDRS Early treatment of diabetic retinopathy study, *SkD* skeleton density, *VD* vessel density, *VDI* vessel diameter index, *SD* standard deviation. *Reproduced under CC BY 4.0, from (1)*

	ETDRS Sectors								
	1	**2**	**3**	**4**	**5**	**6**	**7**	**8**	**9**
SkD Mean (SD)	0.012 (0.014)	0.047 (0.03)	0.044 (0.026)	0.05 (0.026)	0.043 (0.027)	0.063 (0.03)	0.087 (0.03)	0.06 (0.026)	0.041 (0.022)
VD Mean (SD)	0.039 (0.047)	0.214 (0.106)	0.181 (0.09)	0.221 (0.09)	0.175 (0.1)	0.302 (0.109)	0.4 (0.095)	0.289 (0.093)	0.19 (0.078)
VDI Mean (SD)	2.983 (0.929)	4.704 (0.926)	4.465 (0.945)	4.85 (1.096)	4.422 (0.899)	5.18 (1.064)	4.881 (1.093)	5.163 (1.165)	5.064 (1.031)

4.1.2. Comparison of the two methods based on VD, SkD, and VDI parameters

Concerning the SkD and VD parameters, MHF generally showed higher median, lower, and upper quartile values compared to ST (Figure 11), except for the VD parameter. Sector 6 showed solely an upper quartile exception, while in sector 7, both the median and upper quartile were higher with ST. Meanwhile, mean values were also generally higher with MHF (except for the VD parameter in sector 7); however, standard deviations were greater with ST.

In contrast, values associated with VDI were notably higher with ST compared to MHF, with the standard deviation remaining notably larger with ST.

Results in sector 1 significantly differed from all other sectors due to the notably low vascular density of the FAZ.

DOI:10.14753/SE.2024.3041

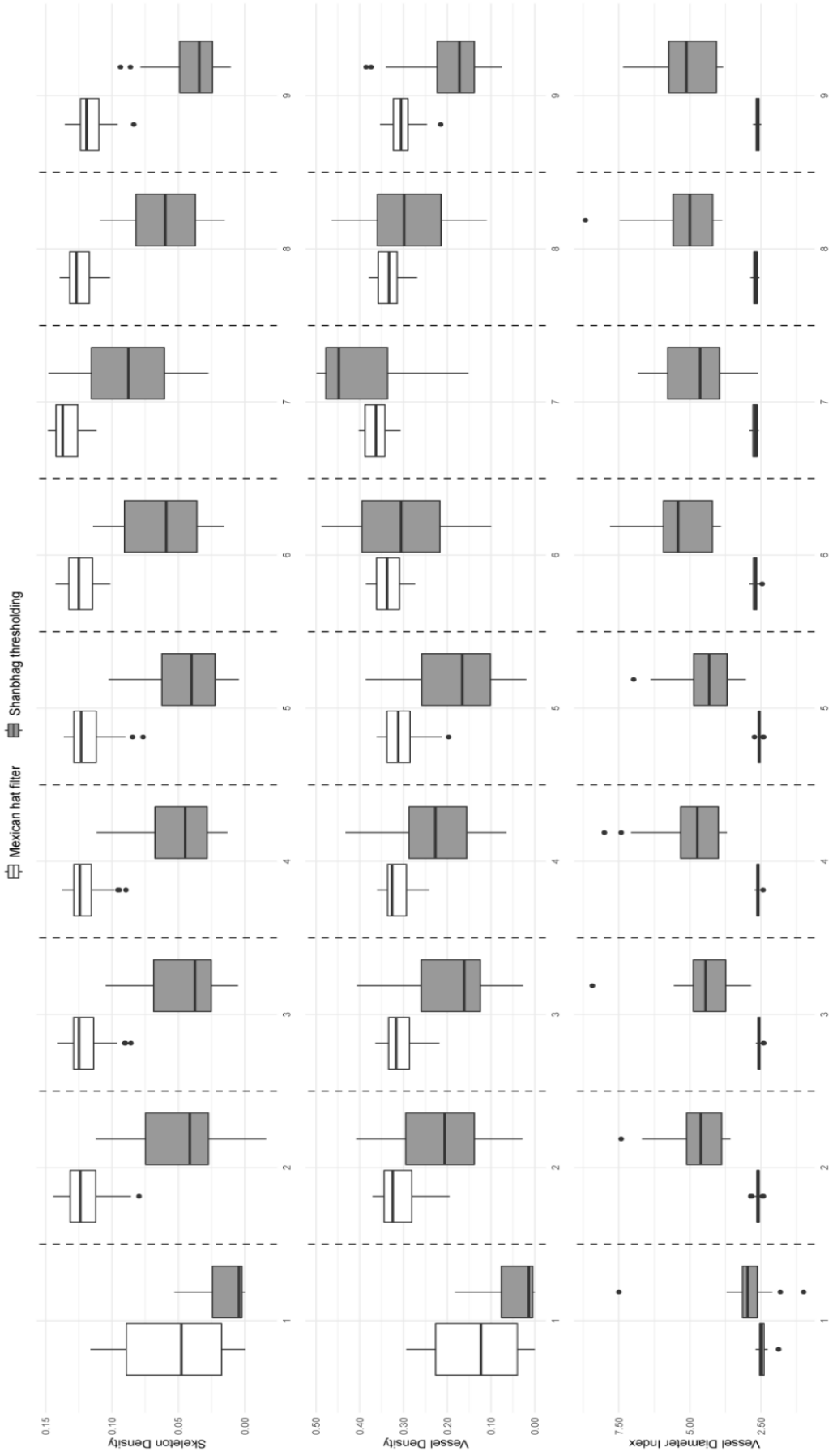

Figure 11. Comparisons of Skeleton Density, Vessel Density, and Vessel Diameter Index parameters with Mexican hat filter and Shanbhag thresholding. Sectors: ETDRS sectors, see Figure 6. for the explanation of those.

In line with the previous descriptive findings, SkD values with MHF were consistently higher than those with ST in the Bland-Altmann plots as well (Figure 12).

Observing the point cloud shape, there was a consistent negative correlation between the mean values and differences of the two methods (except for sector 1). Higher means indicate smaller differences, with the lower limit of agreement near zero in sector 7 and at zero only in sector 1. The mean of differences was significantly different from zero across all sectors per the 95% confidence interval.

In terms of the VD parameter, the pattern of differences was less uniform (Figure 13). Sectors 2, 3, 4, 5, and 9 showed a negative correlation between means and differences. However, in sectors 6, 7, and 8, MHF values were higher for lower means, while ST values were higher than MHF for higher means. Except for sector 7, the mean of differences was positive (consistent with the boxplots) in every sector, with the lower limit of agreement containing zero in almost every sector. Nevertheless, the 95% confidence interval showed that the mean of differences was significantly different from zero in all sectors.

Regarding the VDI parameter, consistent with earlier findings, ST values were higher than those of MHF, with differences in the negative range (Figure 14).

Overall, considering the shape of the point cloud, a negative correlation exists between mean measurements and differences for the two methods. Except for sector 1, the upper limit of agreement did not contain zero in any sector. Based on the 95% confidence interval, the mean of differences was significantly different from zero across all sectors.

DOI:10.14753/SE.2024.3041

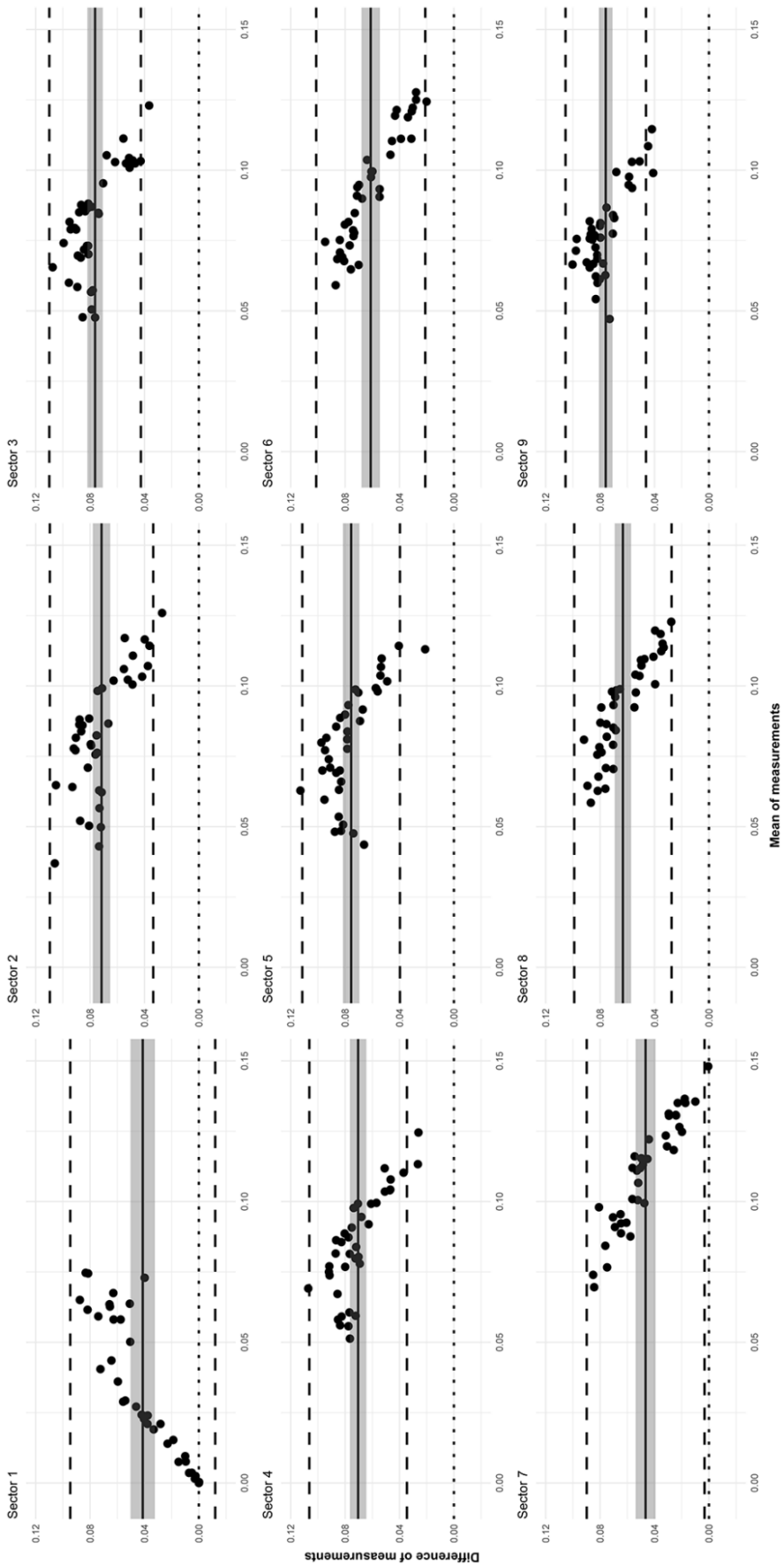

Figure 12. Mexican hat filter and Shanbhag thresholding comparison using the SkD parameter. Bland–Altman plots in the 9 ETDRS sectors (see Figure 3. for the explanation of the sectors). The x axis represents the mean of measurements, the y axis represents the difference of measurements for each graph, individually. The solid line indicates the mean of the differences; the shade around the solid line indicates the 95% confidence interval of mean difference; the upper and lower dashed lines indicate the upper and lower limits of agreement (LA), whereas the dotted line indicates zero.

DOI:10.14753/SE.2024.3041

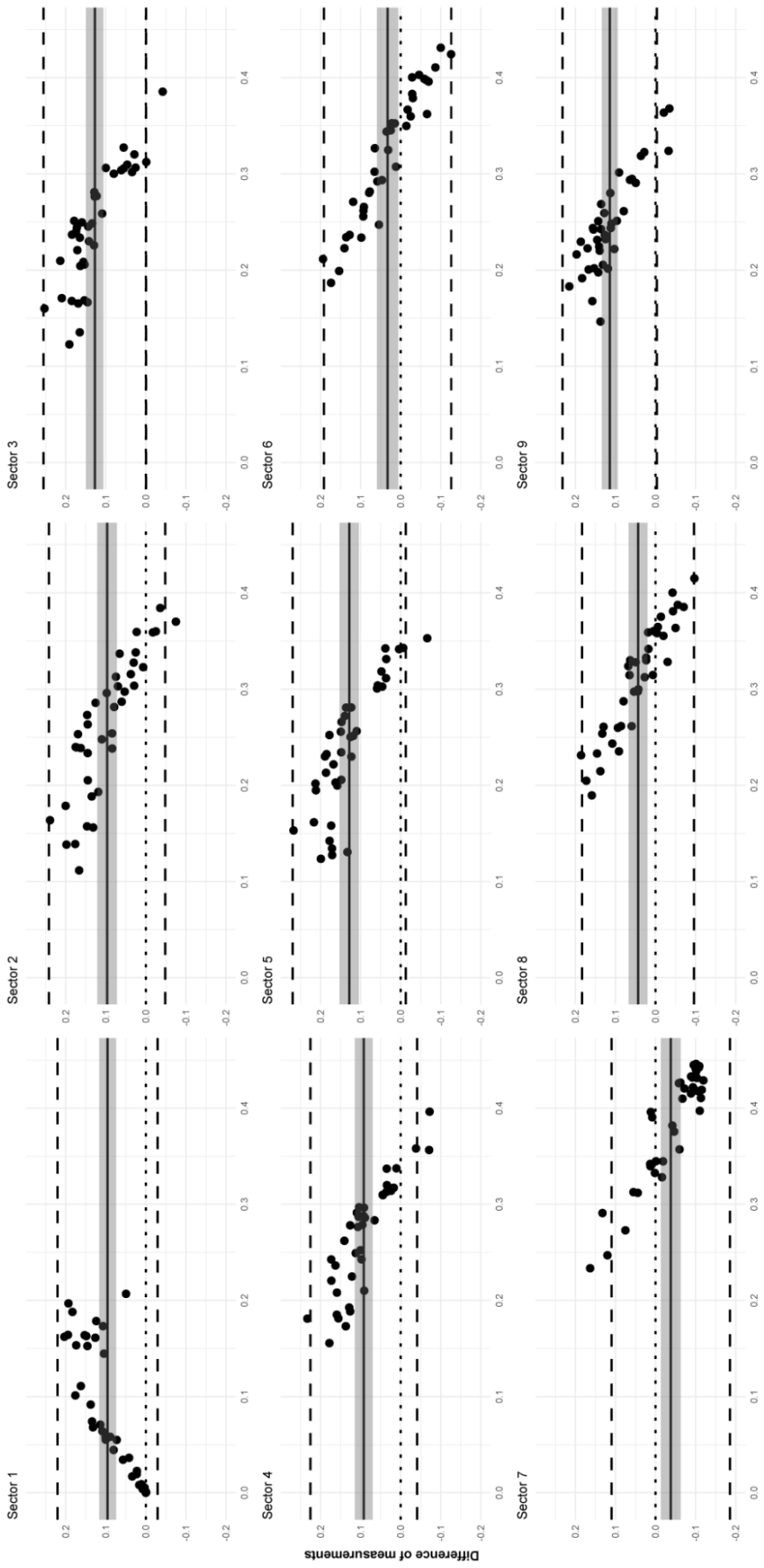

Figure 13. Mexican hat filter and Shanbhag thresholding comparison using the VD parameter. Bland–Altman plots in the 9 ETDRS sectors (see Figure 3 for the explanation of the sectors). The x axis represents the mean of measurements, the y axis represents the difference of measurements for each graph, individually. The solid line indicates the mean of the differences; the shade around the solid line indicates the 95% confidence interval of mean difference; the upper and lower dashed lines indicate the upper and lower limits of agreement (LA), whereas the dotted line indicates zero. *Reproduced under CC BY 4.0 from (1)*

DOI:10.14753/SE.2024.3041

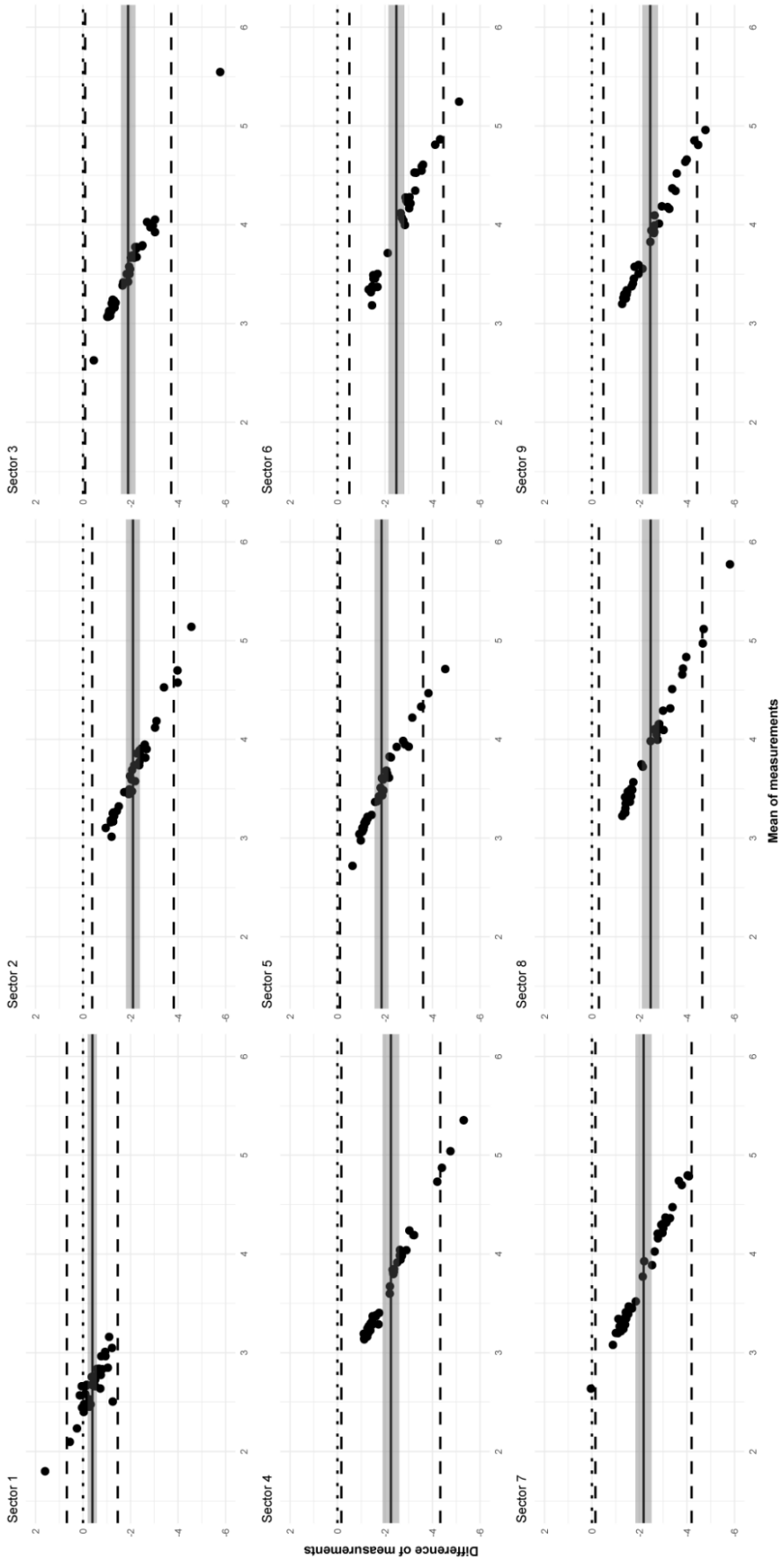

Figure 14. Mexican hat filter and Shanbhag thresholding comparison using the VDI parameter. Bland–Altman plots in the 9 ETDRS sectors (see Figure 3 for the explanation of the sectors). The x axis represents the mean of measurements, the y axis represents the difference of measurements for each graph, individually. The solid line indicates the mean of the differences; the shade around the solid line indicates the 95% confidence interval of mean difference; the upper and lower dashed lines indicate the upper and lower limits of agreement, and the dotted line indicates zero. *Reproduced under CC BY 4.0 from (1)*

DOI:10.14753/SE.2024.3041

4.2. Comparison of OCTA, fluorescein angiography, and indocyanine green angiography images in patients with age-related macular degeneration

4.2.1. FAZ area, perimeter, and circularity in FA and SS-OCTA

Twenty-four eyes were included in the comparison between FA and SS-OCTA. However, three eyes had to be excluded due to the inability to capture adequate FA images displaying all details of the FAZ.

The mean FAZ area measured by FA and SS-OCTA was 0.26 ± 0.12 mm² and 0.26 ± 0.11 mm², respectively (P = 0.96, r = 0.933). The FAZ perimeter showed no significant difference between FA and SS-OCTA delineations (P = 0.29), measuring 2.1 ± 0.59 mm and 2.1 ± 0.56 mm, respectively. However, a statistically significant difference was noted in FAZ circularity. The mean FAZ circularity in FA was 0.71 ± 0.12 and 0.68 ± 0.11 in SS-OCTA, with a P-value of 0.047. The difference between FA and SS-OCTA FAZ circularity was 3.4 ± 8.3%.

Using the Bland–Altman method for comparison, a bias of 0.0004 ± 0.04 mm² was observed between SS-OCTA and FA for FAZ area, indicating an excellent level of agreement. The FAZ perimeter and circularity displayed biases of 0.04 ± 0.19 and -0.03 ± 0.06, respectively.

4.2.2. CNV lesion size, perimeter, and circularity in ICGA and SS-OCTA

Twenty eyes were considered for a comparison between ICGA and SS-OCTA. The mean sizes of CNV lesions measured with ICGA and SS-OCTA were 1.60 ± 1.63 mm² and 1.50 ± 1.48 mm², respectively (P = 0.053, r = 0.992). There were no statistically significant differences observed between the ICGA and SS-OCTA CNV lesion perimeters, which measured 4.9 ± 3.1 mm and 4.8 ± 3.0 mm, respectively. Similarly, CNV circularity did not show a statistically significant difference between ICGA (0.65 ± 0.14) and SS-OCTA (0.64 ± 0.12) with a P-value of 0.386. Bland–Altman analysis revealed a negative bias across all comparisons between ICGA and SS-OCTA. Specifically, choroidal neovascularization lesion size, perimeter, and circularity displayed biases of -0.10 ± 0.24 mm², -0.12 ± 0.55 mm, and -0.02 ± 0.08 mm.

DOI:10.14753/SE.2024.3041

4.3. Detecting microvascular and morphological changes in eyes with central retinal non-perfusion

Forty-four patients (17 females) contributed a total of 44 eyes to the study. Twenty-two eyes had DR and 22 eyes had RVO. Among the RVO cases, seven eyes (32%) had central retinal vein occlusion (CRVO), and 15 eyes (68%) had branch retinal vein occlusion (BRVO). The diabetic cohort consisted of 2 eyes with mild DR (9%), 3 eyes with moderate DR (13%), 4 eyes with severe DR (18%), and 13 eyes with proliferative DR/ proliferative DR after treatment (anti-VEGF injections, laser photocoagulation or vitrectomy) (59%), categorized based on the ETDRS scale.

The average age of the study participants was 60.55±11.38 years; mean decimal BCVA was 0.8 ± 0.36 (Snellen 20/25).

Only 3 patients (7%) had not undergone previous treatment for their retinal condition. Among those who had received prior treatment, 75% had undergone treatment for macular edema, and 24% had received treatment for proliferative diabetic retinopathy (DR).

Approximately 75% of the patients had previously been treated with anti-VEGF medications (Aflibercept, Eylea, Bayer, Germany), but none had received injections for at least two months prior to their inclusion in the study. The average number of anti-VEGF injections was 5.2 for patients with retinal vein occlusion (RVO) and 2.0 for patients with diabetic retinopathy (DR).

Furthermore, 30% of DR patients had undergone laser photocoagulation, while 6% had undergone vitrectomy due to vitreous hemorrhage, tractional retinal detachment, or epiretinal membrane. Additionally, 11% of the participants had undergone cataract surgery.

4.3.1. Wide-field fluorescein angiography results

We identified peripheral retinal ischemia using wide-field fluorescein angiography. Among the twenty-two RVO patients, 20 had interpretable wide-field angiographies. Among these, six patients (30%) displayed no peripheral nonperfusion. Nine patients (40%) exhibited nonperfusion areas of ≤5 disc diameters, while five patients (25%) had nonperfusion areas exceeding 5 disc diameters.

In the case of DR patients, three patients (21%) showed no signs of peripheral nonperfusion. Among the remaining DR patients, eight (67%) displayed nonperfusion areas of ≤5 disc diameters, and two patients (14%) exhibited nonperfusion areas exceeding 5 disc diameters. Twelve DR patients had either inconclusive or ungradable angiographies.

This distribution indicated comparability between the two patient groups, suggesting that the extent of peripheral ischemia likely did not influence the outcomes.

4.3.2. Comparison of BRVO and CRVO, NPDR and PDR groups

We conducted a comparison between BRVO and CRVO patients, and we have found that patients with BRVO exhibited a notably higher count of collateral vessels in the DCP ($p = 0.014$). To conduct further statistical analysis, we combined these two groups into a unified RVO category.

However, due to the limited number of cases with mild ($n = 2$), moderate ($n = 4$), and severe ($n = 3$) DR, we opted to create two distinct groups (NPDR and PDR) to assess whether there were variations in parameter distribution based on DR severity. Following Bonferroni correction, we found no statistically significant differences between these two groups.

4.3.3. Comparison of DR and RVO groups

Patients with DR exhibited significantly higher occurrences of microaneurysms (MAs) ($p = 0.007$) and epiretinal membranes (ERM) ($p = 0.007$). However, no

statistically significant differences were observed between the DR and RVO groups concerning age (p = 0.55), best-corrected visual acuity (BCVA) (p = 0.77), foveal avascular zone (FAZ) (p>1), disorganization of the retinal inner layers (DRIL) (p = 0.54), hyperreflective foci (HRF) (p = 0.37), collateral vessels of the superficial capillary plexus (SCP) (p = 0.66) or deep capillary plexus (DCP) (p = 0.88), disruption of the ellipsoid zone (EZ) (p = 0.73), disruption of the external limiting membrane (ELM) (p = 0.33), or vessel parameters. (Table 3) Notably, the number of prior anti-VEGF injections was significantly higher in the RVO group compared to the DR group (p < 0.001).

Table 3. Summary of the vessel variables with the p- values, showing the differences between DR and RVO groups.

Reproduced under CC BY 4.0, from (28)

Vascular characteristics	**DR group Mean± SD**	**RVO group Mean± SD**	**All patients Mean± SD**	**P value**
Vessel area (mm^2)	10.27± 1.22	10.79± 1.62	10.52± 1.47	0.24
Vessel density (%)	28.8± 3.43	30.25± 4.51	29.52± 4.12	0.25
Average vessel length (mm)	5.21± 1.77	6.58± 2.64	5.89± 2.38	0.06
Total number of junctions	350.36 ± 52.28	354.4± 70.16	352.39± 62.62	0.83
Junction density (%)	9.83 ± 1.46	9.93± 1.95	9.88± 1.75	0.84
Total vessel length (mm)	2.73 ± 0.23	2.76± 0.31	2.75± 0.28	0.57
Number of end points	318.73 ± 32.1	310.36± 45.7	314.5± 40.	0.72
Mean lacunarity	0.091± 0.02	0.097± 0.04	0.094± 0.35	0.88
FAZ area (mm^2)	0.45± 0.39	0.45± 0.44	0.45± 0.42	0.68

DOI:10.14753/SE.2024.3041

4.3.4. Descriptive statistics from all patients

Patients across all underlying diseases were combined into a single group for a descriptive assessment of OCT and OCTA parameters, correlating these findings with BCVA. Results showed varying prevalence among patients with retinal ischemia: DRIL was present in 53%, HRF in 36%, ELM disruption in 68%, EZ disruption in 73%, and IRC in 50%. Collateral vessels in the SCP and DCP were observed in 14% and 25% of ischemic patients, respectively. MAs were found in 43% of all patients, while ERM occurred in 41%.

The correlation between BCVA and most parameters did not reach statistical significance (age: $p = 0.063$, $r = -0.347$; VD: $p = 0.123$, $r = 0.31$; all others $p>1$). A negative correlation was found between FAZ and BCVA ($p = 0.045$, $r = -0.365$). For DR and RVO groups separately, FAZ showed a similar trend: higher FAZ correlated with poorer visual acuity. However, these correlations did not reach statistical significance when analyzed individually (DR group: $r = -0.341$, $p = 0.12$; RVO group: $r = -0.309$, $p = 0.16$).

DOI:10.14753/SE.2024.3041

5. Discussion

5.1. Analysis of retinal vascular density on OCTA images of healthy subjects using two semi-manual methods

In recent years, there has been a growing interest in analyzing retinal vessel density (VAD) using OCTA images. Prior to the emergence of automated VAD analysis programs, multiple studies assessed the pros and cons of various VAD quantification tools and OCTA devices. (61-64, 68-70, 82) Moreover, additional software programs like MATLAB, ImageJ, and Angiotool facilitate semi-manual VAD measurements on binarized and/or skeletonized OCTA images, frequently used in ophthalmological research. However, the lack of standardized segmentation and layer definitions across these studies poses a significant challenge and limits the accuracy and comparability of these measurements.

Our research focused on the comparison of retinal vascular measurements in healthy individuals by using two distinct post-processing approaches on images acquired from the same OCTA system. The initial method utilized MHF and drew inspiration from a prior study conducted by Kim et al. (63)

MHF, a top-hat filter, enables measurements of vascular density and diameter, frequently employed in ophthalmological studies focusing on VAD assessment. (63, 74, 75) We chose this technique as a basis for comparison.

ST, introduced by Shanbhag, has been referenced in a single paper (81) for OCTA image processing among numerous thresholding techniques, receiving limited attention thus far. It was previously featured in only two medical papers, primarily for assessing nerve echogenicity (121) and dermatoscopy images (122). Our research team opted to compare this latter technique to explore its potential clinically relevant advantages, as elaborated below.

MHF and ST methods differ significantly in their approach. MHF relies on an overall image-derived grey level threshold, applying a fixed threshold to classify pixel brightness relative to this threshold. Conversely, ST evaluates each pixel's surroundings to determine its brightness, utilizing a dynamic threshold. Consequently, MHF might reveal slightly more capillaries than otherwise visible in the original OCTA image, creating a more

regular vascular network. In contrast, ST emphasizes larger vessels, making them appear sharper and thicker while causing some capillaries to disappear, resulting in more black areas in the ST binarized images. (1)

Before this study, our team experimented with various post-processing techniques using the ImageJ software in a preliminary pilot. During our exploration, we recognized ST as a promising candidate due to its potential to visualize capillary drop-out in affected areas more effectively compared to MHF. (1) However, a validation on a patient cohort with retinal pathology would be required to confirm our observation.

While MHF might initially seem to represent the anatomical vascular network more realistically, both methods might generate image artifacts during binarization. The noise filter function of both methods has nearly identical efficiency but with opposite effects: MHF shows more capillaries than there are in reality (false flow), while ST eliminates certain capillaries (flow void). (1)

Upon comparing the binarized images to the original, it appears that the production of artifacts differs: MHF generates considerably fewer false flows compared to the flow voids resulting from ST, and the images binarized by MHF seemed more similar to the original OCTA images than those processed by ST. (1) However, this observation is based solely on our assessment, as the actual VAD remains unknown.

While utilizing MHF, manual outlining of the FAZ is necessary, whereas ST automatically eliminates it. Notably, the FAZ identified by ST appeared larger than the manually outlined FAZ using MHF in our OCTA images. (1) This discrepancy stems from the differing thresholding methods. However, our examination focused on young, healthy individuals with normal vascular networks and FAZ sizes, it is important to note that the manually selected FAZ shape seemed more similar to the FAZ on the original image than that selected by ST. Nevertheless, we have to notice that our study did not focus on FAZ measurements; thus, these observations remain qualitative.

Furthermore, we assessed the impact of both techniques on the continuity of the vascular network. We hypothesized that less fragmentation in binarized OCTA images corresponds more closely to actual anatomy. MHF generated more fragmented segments compared to ST. (1)

Based on our above detailed observations, it proves challenging to offer a definitive response regarding the superior suitability of either method for assessing vascular density.

As previously mentioned, our study involved healthy participants only, and without comparisons across different patient groups, it is challenging to definitively recommend ST over MHF or vice versa. Nonetheless, we speculate that MHF might offer advantages in cases involving pathologies affecting the FAZ, while utilizing ST may be beneficial in studies that compare eyes exhibiting reduced retinal VAD with those of healthy eyes. (1)

Cole et al. (123) propose vessel density as a potential surrogate endpoint for future clinical trials. Yet, in a recent commentary, Garrity and Sarraf (124) emphasized the necessity for further technical and clinical research to thoroughly understand the properties and reliability of quantitative indices before their adoption in research trials and clinical settings. Existing evidence indicates promising intra- and inter-operator repeatability of vessel density in images acquired under consistent conditions—same location, angiocube size, machine, and quantification algorithm. (125-127)

Cross-comparisons between semi-automated and automated programs prove challenging due to distinct algorithms and nomenclature. Achieving standardization in these algorithms and programs appears unlikely in the near future, primarily due to the diverse technologies employed by numerous manufacturers. Unfortunately, the absence of a gold standard for VAD analysis, lack of consensus in literature, and absence of unified terminology for investigated parameters add to the complexity.

Munk et al. (128) have undertaken efforts to establish a consensus on nomenclature for OCTA findings in retinal vascular diseases. While progress has been made in several areas of VAD measurement, discussions highlight the persisting confusion in nomenclature describing OCTA-based quantification. The need for uniform terminology across different manufacturers' software programs remains evident.

Moreover, creating a robust normative database for vascular density measurements in healthy subjects presents a formidable challenge, given the previously outlined differences. Tan et al., in a recent publication (129), presented a normative database involving 138 healthy Asian subjects, categorized into four age groups, based on 12×12 mm OCTA images. Their methodology utilized a swept-source OCT system, employing U-NET, a deep learning architecture, for segmenting large vessels and a moving window scheme for capillary segmentation. However, it is important to note that a normative database can only provide guidance for the evaluation of images taken with the same type of device and of the same OCTA image size. (130)

The current study has several limitations worth noting. Firstly, our analysis of vascular density parameters centered on the two semi-manual methods mentioned, lacking comparisons with alternative quantification tools. Additionally, our inclusion of a relatively small number of healthy participants suggests the need for validation on larger cohorts. To ascertain clinically significant differences, future cohorts should include individuals with retinal pathology.

5.2. Comparison of OCTA, fluorescein angiography, and indocyanine green angiography images in patients with age-related macular degeneration

The routinely used clinical angiography methods are fluorescein angiography (FA) for examining the retina and indocyanine green angiography (ICGA) for the choroid. Despite their success, both FA and ICGA are invasive, time-consuming, and pose potential risks of allergic reactions due to the dyes. (131) FA focuses solely on the superficial retinal circulation in a two-dimensional manner, lacking the capability to visualize deeper capillary structures, while ICGA predominantly serves choroid imaging. (22) These limitations led to the pursuit of faster, safer imaging tools capable of effectively capturing both retinal and choroidal circulations, such as optical coherence tomography angiography.

Our research team, along with other groups, have published studies comparing OCTA with ICGA (93-95) or OCTA with FA (88, 89) imaging. These comparisons aimed to deepen our comprehension of the visualizations provided by the non-invasive and dye-free OCTA technology. However, none of these studies incorporated image registration or any alternative method to address image distortions arising from factors such as recording angle variations, eye movements, or optical aberrations.

As far as we know, this study represents the first attempt to utilize a deep-learning-assisted image registration algorithm prior to conducting measurements comparisons across various angiography techniques.

Our prior research demonstrated a statistically significant discrepancy in CNV lesion size between SD-OCTA and ICGA for both Type 1 and Type 2 nAMD. (95) A recent study reaffirmed these earlier observations for Type 1 nAMD, noting a statistically

significant larger CNV area in ICGA compared to SD and SS-OCTA. (93) Moreover, investigations into Type 1 nAMD revealed that CNV lesions were statistically larger in ICGA than in SD-OCTA. (94) The disparity in lesion size between the two imaging techniques was estimated to range from a 4.5% to 18.4% underestimation in SD-OCTA. (90, 95) A similar trend was observed in polypoidal choroidal vasculopathy, where lesions appeared smaller in SD-OCTA than in ICGA. (132) These differences have been attributed to various factors such as potential overestimation by ICGA due to dye leakage, potential underestimation by OCTA due to signal attenuation by RPE, or variations in the wavelength used to determine the minimum detectable flow. The wavelength hypothesis finds support in reports indicating higher CNV detection rates with SS-OCTA compared to SD-OCTA, as well as larger CNV lesion sizes observed with SS-OCTA than with SD-OCTA. (85, 133, 134)

In our investigation, we utilized SS-OCTA in patients with treatment-naïve nAMD for comparative analysis. We made a deliberate effort to exclude areas affected by dye leakage around CNV lesions to mitigate potential overestimation observed in ICGA. Additionally, our analysis extended beyond evaluating lesion size; we analyzed parameters like perimeter and circularity to get deeper insight into lesion characteristics. These additional metrics aimed to capture potential disparities, despite the expectation of concordance in CNV and FAZ area measurements across imaging systems. It is important to note, that we did not use the Littman formula (135, 136) to define the real size of the measured areas. Inclusion criteria of the patients was the maximum refractive error ± 6 diopters (spherical equivalent), and we did not measure the axial length of the patients' eyes.

Utilizing a deep-learning-assisted technique for image registration, our study shows absence of statistically significant differences in CNV lesion area between SS-OCTA and ICGA ($P > 0.05$). The correlation analysis revealed a strong agreement in measurements ($r = 0.992$). Using the Bland–Altman method for comparison, a negative bias of -0.1 ± 0.24 mm^2 was observed, indicating slightly smaller CNV areas in SS-OCTA compared to ICGA, with respective areas of 1.50 ± 1.48 mm^2 and 1.60 ± 1.63 mm^2 ($P = 0.053$). Additionally, there was no statistically significant difference observed in choroidal neovascularization perimeter and circularity, emphasizing the importance of prior image registration.

Research conducted on diabetic patients has consistently indicated a notably larger FAZ area in FA compared to OCTA. On the other hand, in patients with retinal vein occlusion, the FAZ appeared larger in SD-OCTA than in FA. However, there has been a lack of available data concerning treatment-naïve nAMD patients in this regard. Our study uncovered a strong correlation between FA and SS-OCTA FAZ size measurements (0.26 ± 0.10 and 0.26 ± 0.11 mm^2, respectively, P = 0.96, r = 0.933). This discrepancy could be attributed to the fact that while patients with diabetes or retinal vein occlusion experience involvement of both the superficial and deep retinal vascular plexus, this might not be the case for Type 1 and 2 nAMD patients.

Upon applying deep-learning-based image registration, our Bland–Altman analysis revealed an extremely low bias of 0.0004 ± 0.04 mm^2 and a mean difference of 1.8%, suggesting a remarkable agreement between these two imaging techniques. However, a statistically significant difference was observed in FAZ circularity. The mean FA FAZ circularity was 0.68 ± 0.11 in SS-OCTA and 0.71 ± 0.12 in FA (P value = 0.047), with a mean percent difference of 3.4 ± 8.3%. This disparity implies that in FA, certain small cavities or gaps within the FAZ might go undetected, resulting in higher circularity values indicating a more rounded FAZ shape. Conversely, in OCTA images, slow blood flow within the small retinal capillaries could lead to undetectable signals, creating cavities or gaps that mimic capillary dropout, subsequently reducing circularity.

To summarize, our findings reveal a high level of agreement between SS-OCTA and ICGA, as well as FA area measurements, in treatment-naïve neovascular AMD patients following the implementation of an innovative deep-learning-based image registration method. This step proves to be essential in comparative analyses and significantly contributes to comprehending the capabilities of SS-OCTA. As a result, we advocate for a shift in the diagnostic approach for nAMD, suggesting the utilization of SS-OCTA angiography and structural data as the primary diagnostic tool, reserving FA/ICGA as secondary options when supplementary information is required.

DOI:10.14753/SE.2024.3041

5.3. Detecting microvascular and morphological changes in eyes with central retinal non-perfusion

The goal of this research was to conduct a quantitative evaluation of OCT and OCTA parameters in patients with DR and RVO experiencing various forms of central retinal ischemia, aiming to establish the relationship between potential biomarkers and visual acuity.

DR continues to stand as a leading cause of visual impairment and blindness globally. (137) Approximately 285 million individuals worldwide are estimated to be affected by diabetes mellitus, underscoring the substantial population at risk for developing DR and associated visual complications. (137) Diagnosing and managing DR presents a significant challenge due to the delayed clinical manifestation of the disease. Typically, in type 2 diabetes mellitus, the clinical presentation of DR emerges 10 to 20 years after the initial diabetes diagnosis. For type 1 diabetes mellitus, this presentation occurs approximately 5 to 10 years following the diagnosis. This delayed onset underscores the difficulty in early detection and intervention, often leading to complications in diagnosis and management. (138)

OCTA offers clinicians a valuable chance to identify ongoing subclinical alterations in DR before the emergence of visible clinical signs and symptoms. Previous studies have successfully shown that OCTA can detect clinically meaningful signs within the macula of individuals with diabetes, providing a means to monitor and detect early changes well before they become clinically evident. (139-144)

Changes at the capillary level have long been observed in individuals with RVO. These alterations manifest as impaired perfusion, vascular dilation, tortuosity, shunting, cotton-wool spots, and retinal hemorrhages, among other clinical findings. (21) Kashani et al., in a pilot study involving 25 subjects with varying RVO severity and controls, demonstrated that OCTA imaging could successfully identify all clinically relevant macular findings associated with RVO. (145) Moreover, this study suggested that findings in the DCP were more pronounced than those in the SCP among individuals with RVO. Several subsequent studies by Rispoli, Savastano et al. (146) and Adhi, Filho et al. (147) have confirmed these findings, providing additional support for the identification and significance of these observed changes in RVO.

In our study, we conducted an analysis on 44 eyes of 44 patients, with 22 affected by RVO and 22 by DR. Our findings highlighted that the FAZ size serves as the most reliable indicator of visual prognosis in individuals experiencing macular nonperfusion. When comparing the two groups of diseases, we observed a significant difference only in the occurrence of MAs and ERM, which were notably more prevalent in DR patients. Other vascular and morphological parameters did not show significant differences between the groups.

Earlier research has indicated that the size and shape of the FAZ can serve as dependable biomarkers, noting an enlargement in the FAZ area compared to healthy controls in both DR and RVO. (101, 148) It should be noted that we did not use the Littman formula (135) (136) to measure the real size of the FAZ. The reason for this was that the patients were selected retrospectively based on OCT angiography images, and they were not recalled for axial length measurements.

In DR, the enlargement of the FAZ stands as one of the initial indicators that notably correlates with both visual acuity and the severity of DR itself. (100, 103, 149) Our findings align with prior research, showing a significant correlation between the FAZ area and BCVA. However, it is important to note that this correlation did not achieve statistical significance when separately comparing FAZ and BCVA within the DR and RVO groups, likely due to the limited sample size, but combining the groups indicates a significant difference due to the larger sample size.

Vessel density has consistently shown significant reduction in both DR and RVO. This reduction has also been observed to correlate with changes in visual acuity. (101, 103) In our study, the correlation observed between VD and BCVA did not achieve statistical significance.

In our current investigation, we evaluated vascular parameters to explore the similarities and distinctions in morphology between central retinal ischemia resulting from DR and RVO. Despite analyzing all vascular parameters, we did not detect statistically significant differences between the two groups. This suggests that the OCTA presentation of ischemia within the retinal microvasculature appears independent of the underlying disease.

Morphological OCT parameters such ELM and EZ disruption, HRF, and DRIL have been identified as markers indicating visual outcomes and ischemic conditions in both

DR and RVO. (99, 120, 150, 151) DRIL offers insights into the status of the inner retinal layers, while disruptions in the EZ and ELM serve as indicators for the outer retinal layers. The EZ specifically represents the inner segment of photoreceptors, enabling deductions about the photoreceptors' condition based on their integrity. Moreover, the integrity of the ELM plays a pivotal role in upholding retinal structure, metabolic processes, and overall homeostasis. (148) Hyperreflective foci have been identified as an early subclinical indicator of barrier breakdown in DR and serve as a prognostic factor for BCVA in cases of RVO. (151, 152) In our study, we did not observe any correlation between DRIL, HRF, ELM, EZ disruption with BCVA.

Collateral vessels in RVO emerge due to altered hemodynamics and heightened hydrostatic pressure. They manifest as twisted or tortuous vessels within the retina or on the optic disc. (153) In our research, we did not find any notable variations in vascular collaterals between the DR and RVO groups. Furthermore, we could not establish a correlation between vascular collaterals and BCVA.

Our study revealed a notably higher occurrence of MAs and ERM in the diabetic group in contrast to patients with RVO. These findings validate earlier observations and indicate that the presence of MAs are specific to diabetes.

In assessing retinal function amid central ischemia, we utilized BCVA as an evaluation measure.

Earlier studies employed various methods, including assessing retinal sensitivity through microperimetry. They discovered significantly reduced retinal sensitivity in areas affected by ischemia. (154) Correlations were established between retinal sensitivity, disease duration, and disruption of the EZ in both DR and RVO. (154-156) This robust association suggests that once ischemia occurs, the functional outcomes appear similar, irrespective of the initial cause of the ischemia.

This study has certain limitations. First, its retrospective nature and the relatively small sample size. The small sample size could also be the reason why, unlike previous studies, we did not find a significant correlation between the most of monitored OCT/OCTA parameters and BCVA. Additionally, grouping patients together irrespective of the occluded vascular segment and severity of DR, although no differences were detected between subgroups, could potentially impact the findings. Moreover, the

DOI:10.14753/SE.2024.3041

unsatisfactory quality of OCTA images for the deep capillary plexus hindered the quantitative evaluation of vascular parameters.

The findings of this study support the notion that the appearance of ischemia in the retinal microvasculature in OCTA imaging is not dependent on the underlying disease and yields similar outcomes once ischemia is present. However, to conclusively affirm these assumptions, larger prospective studies using higher-resolution imaging of both retinal vascular plexuses are warranted.

DOI:10.14753/SE.2024.3041

6. Conclusions

Based on our results, the following can be concluded:

1. Analyzing retinal vascular density of healthy individuals, both MHF and ST methods enabled the segmentation of the vascular network and the analysis of vascular density parameters. In terms of the assessed vascular parameters, the two methods generated largely inconsistent results. This implies that they should not be used interchangeably in analysis or interpretation. Additional research is necessary to ascertain the clinical significance of these inconsistent outcomes and to identify which algorithm is superior since there is no definitive gold standard for vascular density analysis and the actual density is unknown. For consistent longitudinal monitoring, it is advisable to utilize the same image processing method.

2. We demonstrated a high level of agreement regarding area measurements between Swept-Source Optical Coherence Tomography Angiography (SS-OCTA), Indocyanine Green Angiography (ICGA), and Fluorescein Angiography (FA) in individuals with treatment-naïve neovascular AMD, by implementing a novel deep-learning-assisted approach for image registration.
   The results suggest a potential shift towards adopting SS-OCTA as the primary diagnostic tool for neovascular age-related macular degeneration. This paradigm shift could redefine diagnostic protocols given its promising performance in this context.

3. In eyes with central retinal non-perfusion, we identified the size of the Foveal Avascular Zone (FAZ) as a key biomarker predicting visual outcomes. While Microaneurysms (MAs) and Epiretinal Membrane (ERM) differed between the groups, other parameters assessed using OCT and OCTA showed similar characteristics in both DR and RVO. This suggests that once retinal ischemia sets in the macular region, its appearance and impact on visual outcomes tends to be consistent regardless of the underlying disease.

DOI:10.14753/SE.2024.3041

7. Summary

In our research, we utilized OCTA technology to measure retinal vessel density in healthy subjects and to investigate disease-specific differences in patients suffering from various retinal diseases. We also compared the OCTA method with other previous imaging technologies.

In the first study, we determined retinal vessel density in OCT angiography images of healthy subjects using two different semi-manual methods. Our study revealed that both MHF and ST techniques facilitated the segmentation of the vascular network and the evaluation of vascular density parameters. However, concerning the evaluated vascular parameters, these two methods produced inconsistent results, meaning they are not interchangeable. Based on our findings and previous studies it can be concluded that for continuous monitoring over time, it is advisable to consistently use the same image processing method.

In the second study, we compared measurements conducted on SS-OCTA, FA, and ICG images of patients with treatment-naïve age-related macular degeneration. Prior to conducting comparisons, we utilized a deep-learning-based image registration technique to account for potential biases caused by image distortions. Our findings indicate a substantial concordance between SS-OCTA, ICGA, and FA area measurements in treatment-naïve patients with neovascular AMD. Our study underscores the crucial role of employing a deep-learning approach in comparative investigations. Consequently, we advocate for a paradigm shift in nAMD diagnostics, suggesting the adoption of SS-OCTA angiography and structural data as the primary diagnostic tool, reserving FA/ICGA as secondary options for supplemental information when necessary.

In our third study, we assessed the features and structural changes related to central retinal ischemia originating from diabetic retinopathy or retinal vein occlusion using OCTA. We also explored their correlation with visual acuity. We found that the most reliable indicator of visual prognosis in diseases with central macular ischemia is the size of the foveal avascular zone. Except for the existence of microaneurysms (MAs) and epiretinal membranes (ERM), all other parameters obtained from OCT and OCTA showed comparable occurrences in both the DR and RVO groups. Our findings suggest that once retinal ischemia occurs within the macular area, its characteristics and visual prognosis remain similar, regardless of the specific underlying disease.

8. References

1. Angeli O, Hajdu D, Jeney A, Czifra B, Nagy BV, Balazs T, Nemoda DJ, Somfai GM, Nagy ZZ, Peto T, Schneider M. Qualitative and quantitative comparison of two semi-manual retinal vascular density analyzing methods on optical coherence tomography angiography images of healthy individuals. Sci Rep. 2023;13(1):16981.

2. Huang D, Swanson EA, Lin CP, Schuman JS, Stinson WG, Chang W, Hee MR, Flotte T, Gregory K, Puliafito CA. Optical coherence tomography. Science. 1991;254(5035):1178-81.

3. Tearney GJ, Brezinski ME, Bouma BE, Boppart SA, Pitris C, Southern JF, Fujimoto JG. In vivo endoscopic optical biopsy with optical coherence tomography. Science. 1997;276(5321):2037-9.

4. Miklos S. Optical coherence tomograpy in ophthalmology. Budapest: Semmelweis Publisher; 2018; 7-14.

5. Podoleanu AG. Optical coherence tomography. J Microsc. 2012;247(3):209-19.

6. de Boer JF, Hitzenberger CK, Yasuno Y. Polarization sensitive optical coherence tomography - a review [Invited]. Biomed Opt Express. 2017;8(3):1838-73.

7. Pircher M, Hitzenberger CK, Schmidt-Erfurth U. Polarization sensitive optical coherence tomography in the human eye. Prog Retin Eye Res. 2011;30(6):431-51.

8. Leitgeb RA, Werkmeister RM, Blatter C, Schmetterer L. Doppler optical coherence tomography. Prog Retin Eye Res. 2014;41(100):26-43.

9. Li Y, Chen J, Chen Z. Advances in Doppler optical coherence tomography and angiography. Transl Biophotonics. 2019;1(1-2).

10. Yang J, Liu L, Campbell JP, Huang D, Liu G. Handheld optical coherence tomography angiography. Biomed Opt Express. 2017;8(4):2287-300.

11. Campbell JP, Nudleman E, Yang J, Tan O, Chan RVP, Chiang MF, Huang D, Liu G. Handheld Optical Coherence Tomography Angiography and Ultra-Wide-Field Optical Coherence Tomography in Retinopathy of Prematurity. JAMA ophthalmology. 2017;135(9):977-81.

12. Sayegh SI, Nolan RM, Jung W, Kim J, McCormick DT, Chaney EJ, Stewart CN, Boppart SA. Comparison of a MEMS-Based Handheld OCT Scanner With a Commercial Desktop OCT System for Retinal Evaluation. Transl Vis Sci Technol. 2014;3(3):10.

13. Battu R, Dabir S, Khanna A, Kumar AK, Roy AS. Adaptive optics imaging of the retina. Indian J Ophthalmol. 2014;62(1):60-5.

14. Jonnal RS, Kocaoglu OP, Zawadzki RJ, Liu Z, Miller DT, Werner JS. A Review of Adaptive Optics Optical Coherence Tomography: Technical Advances, Scientific Applications, and the Future. Investigative ophthalmology & visual science. 2016;57(9):OCT51-68.

15. Pircher M, Zawadzki RJ. Review of adaptive optics OCT (AO-OCT): principles and applications for retinal imaging [Invited]. Biomed Opt Express. 2017;8(5):2536-62.

16. Told R, Reiter GS, Orsolya A, Mittermüller TJ, Eibenberger K, Schlanitz FG, Arikan M, Pollreisz A, Sacu S, Schmidt-Erfurth U. Swept source optical coherence tomography angiography, fluorescein angiography, and indocyanine green angiography comparisons revisited: Using a Novel Deep-Learning-Assisted Approach for Image Registration. Retina (Philadelphia, Pa). 2020;40(10):2010-7.

17. Dahrouj M, Miller JB. Artificial Intelligence (AI) and Retinal Optical Coherence Tomography (OCT). Semin Ophthalmol. 2021;36(4):341-5.

18. Hormel TT, Hwang TS, Bailey ST, Wilson DJ, Huang D, Jia Y. Artificial intelligence in OCT angiography. Prog Retin Eye Res. 2021;85:100965.

19. Ting DSW, Pasquale LR, Peng L, Campbell JP, Lee AY, Raman R, Tan GSW, Schmetterer L, Keane PA, Wong TY. Artificial intelligence and deep learning in ophthalmology. Br J Ophthalmol. 2019;103(2):167-75.

20. Javed A, Khanna A, Palmer E, Wilde C, Zaman A, Orr G, Kumudhan D, Lakshmanan A, Panos GD. Optical coherence tomography angiography: a review of the current literature. J Int Med Res. 2023;51(7):3000605231187933.

21. Kashani AH, Chen CL, Gahm JK, Zheng F, Richter GM, Rosenfeld PJ, Shi Y, Wang RK. Optical coherence tomography angiography: A comprehensive review of current methods and clinical applications. Progress in Retinal and Eye Research. 2017;60:66-100.

22. de Carlo TE, Romano A, Waheed NK, Duker JS. A review of optical coherence tomography angiography (OCTA). Int J Retina Vitreous. 2015;1:5.

23. Waheed NK, Rosen RB, Jia Y, Munk MR, Huang D, Fawzi A, Chong V, Nguyen QD, Sepah Y, Pearce E. Optical coherence tomography angiography in diabetic retinopathy. Prog Retin Eye Res. 2023;97:101206.

24. Ebrahimi B, Le D, Abtahi M, Dadzie AK, Lim JI, Chan RVP, Yao X. Optimizing the OCTA layer fusion option for deep learning classification of diabetic retinopathy. Biomed Opt Express. 2023;14(9):4713-24.

25. Yuan M, Wang W, Kang S, Li Y, Li W, Gong X, Xiong K, Meng J, Zhong P, Guo X, Wang L, Liang X, Lin H, Huang W. Peripapillary Microvasculature Predicts the Incidence and Development of Diabetic Retinopathy: An SS-OCTA Study. Am J Ophthalmol. 2022;243:19-27.

26. Taylor TRP, Menten MJ, Rueckert D, Sivaprasad S, Lotery AJ. The role of the retinal vasculature in age-related macular degeneration: a spotlight on OCTA. Eye (Lond). 2023.

27. Perrott-Reynolds R, Cann R, Cronbach N, Neo YN, Ho V, McNally O, Madi HA, Cochran C, Chakravarthy U. The diagnostic accuracy of OCT angiography in naive and treated neovascular age-related macular degeneration: a review. Eye (Lond). 2019;33(2):274-82.

28. Hajdu D, Told R, Angeli O, Weigert G, Pollreisz A, Schmidt-Erfurth U, Sacu S. Identification of microvascular and morphological alterations in eyes with central retinal non-perfusion. PLoS One. 2020;15(11):e0241753.

29. An W, Han J. Research progress of UWFFA and OCTA in retinal vein occlusion: A review. Eur J Ophthalmol. 2021;31(6):2850-5.

30. Angeli O, Nagy ZZ, Schneider M. [Spontaneous visual recovery following a central retinal artery occlusion in a patient with a cilioretinal artery]. Orv Hetil. 2019;160(29):1146-52.

31. Chen L, Yuan M, Sun L, Wang Y, Chen Y. Evaluation of microvascular network with optical coherence tomography angiography (OCTA) in branch retinal vein occlusion (BRVO). BMC ophthalmology. 2020;20(1):154.

32. Hirano Y, Suzuki N, Tomiyasu T, Kurobe R, Yasuda Y, Esaki Y, Yasukawa T, Yoshida M, Ogura Y. Multimodal Imaging of Microvascular Abnormalities in Retinal Vein Occlusion. J Clin Med. 2021;10(3).

33. Mejía ME, Ríos HA, Rosenstiehl S, Rodríguez FJ. Optical coherence tomography angiography as predictor of visual outcomes in retinal vein occlusion treated with antiangiogenic therapy. Eur J Ophthalmol. 2023;33(1):434-40.

34. Huemer J, Khalid H, Wagner SK, Nicholson L, Fu DJ, Sim DA, Patel PJ, Balaskas K, Rajendram R, Keane PA. Phenotyping of retinal neovascularization in ischemic retinal vein occlusion using wide field OCT angiography. Eye (Lond). 2021;35(10):2812-9.

35. Arya M, Sorour O, Chaudhri J, Alibhai Y, Waheed NK, Duker JS, Baumal CR. Distinguishing intraretinal microvascular abnormalities from retinal neovascularization using optical coherence tomography angiography. Retina (Philadelphia, Pa). 2020;40(9):1686-95.

36. You QS, Guo Y, Wang J, Wei X, Camino A, Zang P, Flaxel CJ, Bailey ST, Huang D, Jia Y, Hwang TS. Detection of clinically unsuspected retinal neovascularization with wide-field optical coherence tomography angiography. Retina (Philadelphia, Pa). 2020;40(5):891-7.

37. Mannil SS, Agarwal A, Conner IP, Kumar RS. A comprehensive update on the use of optical coherence tomography angiography in glaucoma. Int Ophthalmol. 2023;43(5):1785-802.

38. Miguel A, Silva A, Barbosa-Breda J, Azevedo L, Abdulrahman A, Hereth E, Abegão Pinto L, Lachkar Y, Stalmans I. OCT-angiography detects longitudinal microvascular changes in glaucoma: a systematic review. Br J Ophthalmol. 2022;106(5):667-75.

39. Zeng Q, Yao Y, Li S, Yang Z, Qu J, Zhao M. Comparison of swept-source OCTA and indocyanine green angiography in central serous chorioretinopathy. BMC ophthalmology. 2022;22(1):380.

40. Zeng Q, Yao Y, Tu S, Zhao M. Quantitative analysis of choroidal vasculature in central serous chorioretinopathy using ultra-widefield swept-source optical coherence tomography angiography. Sci Rep. 2022;12(1):18427.

41. Pichi F, Hay S. Use of optical coherence tomography angiography in the uveitis clinic. Graefe's archive for clinical and experimental ophthalmology = Albrecht von Graefes Archiv fur klinische und experimentelle Ophthalmologie. 2023;261(1):23-36.

42. Herbort CP, Takeuchi M, Papasavvas I, Tugal-Tutkun I, Hedayatfar A, Usui Y, Ozdal PC, Urzua CA. Optical Coherence Tomography Angiography (OCT-A) in Uveitis: A Literature Review and a Reassessment of Its Real Role. Diagnostics (Basel). 2023;13(4).

43. Fernández-Espinosa G, Boned-Murillo A, Orduna-Hospital E, Díaz-Barreda MD, Sánchez-Cano A, Bielsa-Alonso S, Acha J, Pinilla I. Retinal Vascularization Abnormalities Studied by Optical Coherence Tomography Angiography (OCTA) in Type 2 Diabetic Patients with Moderate Diabetic Retinopathy. Diagnostics (Basel). 2022;12(2).

44. Ong CJT, Wong MYZ, Cheong KX, Zhao J, Teo KYC, Tan TE. Optical Coherence Tomography Angiography in Retinal Vascular Disorders. Diagnostics (Basel). 2023;13(9).

45. Khatri A, Pandey A, Joshi K, Singh K, Prasai G, Pradhan E, Agrawal R. Redefining response in wet AMD to anti VEGF therapy based on non-OCTA versus OCTA evaluation. Eur J Ophthalmol. 2022;32(5):2719-25.

46. Chouhan S, Kalluri Bharat RP, Surya J, Mohan S, Balaji JJ, Viekash VK, Lakshminarayanan V, Raman R. Preliminary Report on Optical Coherence Tomography Angiography Biomarkers in Non-Responders and Responders to Intravitreal Anti-VEGF Injection for Diabetic Macular Oedema. Diagnostics (Basel). 2023;13(10).

47. Or C, Sabrosa AS, Sorour O, Arya M, Waheed N. Use of OCTA, FA, and Ultra-Widefield Imaging in Quantifying Retinal Ischemia: A Review. Asia Pac J Ophthalmol (Phila). 2018;7(1):46-51.

48. Lee WD, Devarajan K, Chua J, Schmetterer L, Mehta JS, Ang M. Optical coherence tomography angiography for the anterior segment. Eye Vis (Lond). 2019;6:4.

49. Chen H, Chi W, Cai X, Deng Y, Jiang X, Wei Y, Zhang S. Macular microvasculature features before and after vitrectomy in idiopathic macular epiretinal membrane: an OCT angiography analysis. Eye (Lond). 2019;33(4):619-28.

50. Cunha-Vaz J. A Central Role for Ischemia and OCTA Metrics to Follow DR Progression. J Clin Med. 2021;10(9).

51. Liu M, Drexler W. Optical coherence tomography angiography and photoacoustic imaging in dermatology. Photochem Photobiol Sci. 2019;18(5):945-62.

52. Xu J, Yuan X, Huang Y, Qin J, Lan G, Qiu H, Yu B, Jia H, Tan H, Zhao S, Feng Z, An L, Wei X. Deep-learning visualization enhancement method for optical coherence tomography angiography in dermatology. J Biophotonics. 2023;16(10):e202200366.

53. Zhang JF, Wiseman S, Valdés-Hernández MC, Doubal FN, Dhillon B, Wu YC, Wardlaw JM. The Application of Optical Coherence Tomography Angiography in Cerebral Small Vessel Disease, Ischemic Stroke, and Dementia: A Systematic Review. Front Neurol. 2020;11:1009.

54. Andleeb F, Katta N, Gruslova A, Muralidharan B, Estrada A, McElroy AB, Ullah H, Brenner AJ, Milner TE. Differentiation of Brain Tumor Microvasculature From Normal Vessels Using Optical Coherence Angiography. Lasers Surg Med. 2021;53(10):1386-94.

55. Tang Y, Liang X, Xu J, Wang K, Jia W. The Value of Optical Coherence Tomography Angiography in Pituitary Adenomas. J Integr Neurosci. 2022;21(5):142.

56. Cennamo G, Solari D, Montorio D, Scala MR, D'Andrea L, Tranfa F, Cavallo LM. The role of OCT- angiography in predicting anatomical and functional recovery after

endoscopic endonasal pituitary surgery: A 1-year longitudinal study. PLoS One. 2021;16(12):e0260029.

57. Monteiro-Henriques I, Rocha-Sousa A, Barbosa-Breda J. Optical coherence tomography angiography changes in cardiovascular systemic diseases and risk factors: A Review. Acta Ophthalmol. 2022;100(1):e1-e15.

58. Lee HC, Ahsen OO, Liang K, Wang Z, Figueiredo M, Giacomelli MG, Potsaid B, Huang Q, Mashimo H, Fujimoto JG. Endoscopic optical coherence tomography angiography microvascular features associated with dysplasia in Barrett's esophagus (with video). Gastrointest Endosc. 2017;86(3):476-84.e3.

59. Deegan AJ, Wang W, Men S, Li Y, Song S, Xu J, Wang RK. Optical coherence tomography angiography monitors human cutaneous wound healing over time. Quant Imaging Med Surg. 2018;8(2):135-50.

60. Men SJ, Chen CL, Wei W, Lai TY, Song SZ, Wang RK. Repeatability of vessel density measurement in human skin by OCT-based microangiography. Skin Res Technol. 2017;23(4):607-12.

61. Chen Y, Laotaweerungsawat S, Zhao T, Haq Z, Liu X, Psaras C, Yang D, Stewart JM. Discordant vascular parameter measurements in diabetic and non-diabetic eyes detected by different optical coherence tomography angiography devices. PLoS One. 2020;15(6):e0234664.

62. Chu Z, Lin J, Gao C, Xin C, Zhang Q, Chen CL, Roisman L, Gregori G, Rosenfeld PJ, Wang RK. Quantitative assessment of the retinal microvasculature using optical coherence tomography angiography. J Biomed Opt. 2016;21(6):66008.

63. Kim AY, Chu Z, Shahidzadeh A, Wang RK, Puliafito CA, Kashani AH. Quantifying Microvascular Density and Morphology in Diabetic Retinopathy Using

Spectral-Domain Optical Coherence Tomography Angiography. Investigative ophthalmology & visual science. 2016;57(9):OCT362-70.

64. Rabiolo A, Gelormini F, Sacconi R, Cicinelli MV, Triolo G, Bettin P, Nouri-Mahdavi K, Bandello F, Querques G. Comparison of methods to quantify macular and peripapillary vessel density in optical coherence tomography angiography. PLoS One. 2018;13(10):e0205773.

65. Coscas F, Sellam A, Glacet-Bernard A, Jung C, Goudot M, Miere A, Souied EH. Normative Data for Vascular Density in Superficial and Deep Capillary Plexuses of Healthy Adults Assessed by Optical Coherence Tomography Angiography. Investigative ophthalmology & visual science. 2016;57(9):OCT211-OCT23.

66. Tomita R, Iwase T, Goto K, Yamamoto K, Ra E, Terasaki H. Correlation between macular vessel density and number of intravitreal anti-VEGF agents for macular edema associated with branch retinal vein occlusion. Sci Rep. 2019;9(1):16388.

67. Capelanes NC, Malerbi FK, Novais EA, Regatieri CVS. Optical Coherence Tomography Angiographic Evaluation of Macular Vessel Density in Diabetic Macular Edema After Intravitreal Dexamethasone Implants: A Prospective Interventional Trial. Ophthalmic Surg Lasers Imaging Retina. 2023;54(3):174-82.

68. Arya M, Rebhun CB, Alibhai AY, Chen X, Moreira-Neto C, Baumal CR, Reichel E, Witkin AJ, Duker JS, Sadda SR, Waheed NK. Parafoveal Retinal Vessel Density Assessment by Optical Coherence Tomography Angiography in Healthy Eyes. Ophthalmic Surg Lasers Imaging Retina. 2018;49(10):S5-S17.

69. Fang D, Tang FY, Huang H, Cheung CY, Chen H. Repeatability, interocular correlation and agreement of quantitative swept-source optical coherence tomography angiography macular metrics in healthy subjects. Br J Ophthalmol. 2019;103(3):415-20.

70. Zhao Q, Yang WL, Wang XN, Wang RK, You QS, Chu ZD, Xin C, Zhang MY, Li DJ, Wang ZY, Chen W, Li YF, Cui R, Shen L, Wei WB. Repeatability and Reproducibility of Quantitative Assessment of the Retinal Microvasculature Using Optical Coherence Tomography Angiography Based on Optical Microangiography. Biomed Environ Sci. 2018;31(6):407-12.

71. Zudaire E, Gambardella L, Kurcz C, Vermeren S. A Computational Tool for Quantitative Analysis of Vascular Networks. PLoS One. 2011;6(11):12.

72. Hosari S, Hohberger B, Theelke L, Sari H, Lucio M, Mardin CY. OCT Angiography: Measurement of Retinal Macular Microvasculature with Spectralis II OCT Angiography - Reliability and Reproducibility. Ophthalmologica. 2020;243(1):75-84.

73. Mehta N, Liu K, Alibhai AY, Gendelman I, Braun PX, Ishibazawa A, Sorour O, Duker JS, Waheed NK. Impact of Binarization Thresholding and Brightness/Contrast Adjustment Methodology on Optical Coherence Tomography Angiography Image Quantification. Am J Ophthalmol. 2019;205:54-65.

74. Akagi T, Uji A, Huang AS, Weinreb RN, Yamada T, Miyata M, Kameda T, Ikeda HO, Tsujikawa A. Conjunctival and Intrascleral Vasculatures Assessed Using Anterior Segment Optical Coherence Tomography Angiography in Normal Eyes. Am J Ophthalmol. 2018;196:1-9.

75. Di Antonio L, Viggiano P, Ferro G, Toto L, D'Aloisio R, Porreca A, Di Nicola M, Mastropasqua R. Retinal vascular metrics difference by comparison of two image acquisition modes using a novel OCT angiography prototype. PLoS One. 2020;15(12):e0243074.

76. Hirano T, Kitahara J, Toriyama Y, Kasamatsu H, Murata T, Sadda S. Quantifying vascular density and morphology using different swept-source optical coherence tomography angiographic scan patterns in diabetic retinopathy. Br J Ophthalmol. 2019;103(2):216-21.

77. Hsiao CC, Yang CM, Yang CH, Ho TC, Lai TT, Hsieh YT. Correlations between visual acuity and macular microvasculature quantified with optical coherence tomography angiography in diabetic macular oedema. Eye (Lond). 2020;34(3):544-52.

78. Kim AY, Rodger DC, Shahidzadeh A, Chu Z, Koulisis N, Burkemper B, Jiang X, Pepple KL, Wang RK, Puliafito CA, Rao NA, Kashani AH. Quantifying Retinal Microvascular Changes in Uveitis Using Spectral-Domain Optical Coherence Tomography Angiography. Am J Ophthalmol. 2016;171:101-12.

79. Liu Z, Wang H, Jiang H, Gameiro GR, Wang J. Quantitative analysis of conjunctival microvasculature imaged using optical coherence tomography angiography. Eye Vis (Lond). 2019;6:5.

80. Shanbhag, G. A. Utilization of information measure as a means of image thresholding, Graph. Models Image Process. (Academic Press, Inc.) 56 (5), 414-419, ISSN: 1049-965-2. 1994.

81. Arrigo A, Aragona E, Saladino A, Amato A, Bandello F, Battaglia Parodi M. The impact of different thresholds on optical coherence tomography angiography images binarization and quantitative metrics. Sci Rep. 2021;11(1):14758.

82. Munk MR, Giannakaki-Zimmermann H, Berger L, Huf W, Ebneter A, Wolf S, Zinkernagel MS. OCT-angiography: A qualitative and quantitative comparison of 4 OCT-A devices. PLoS One. 2017;12(5):14.

83. Huang D, Jia Y, Rispoli M, Tan O, Lumbroso B. Optical coherence tomography angiography of time course of choroidal neovascularization in response to anti-angiogenic treatment. Retina (Philadelphia, Pa). 2015;35(11):2260-4.

84. Coscas G, Lupidi M, Coscas F, Français C, Cagini C, Souied EH. Optical coherence tomography angiography during follow-up: qualitative and quantitative

analysis of mixed type I and II choroidal neovascularization after vascular endothelial growth factor trap therapy. Ophthalmic Res. 2015;54(2):57-63.

85. Told R, Ginner L, Hecht A, Sacu S, Leitgeb R, Pollreisz A, Schmidt-Erfurth U. Comparative study between a spectral domain and a high-speed single-beam swept source OCTA system for identifying choroidal neovascularization in AMD. Sci Rep. 2016;6:38132.

86. Moult E, Choi W, Waheed NK, Adhi M, Lee B, Lu CD, Jayaraman V, Potsaid B, Rosenfeld PJ, Duker JS, Fujimoto JG. Ultrahigh-speed swept-source OCT angiography in exudative AMD. Ophthalmic Surg Lasers Imaging Retina. 2014;45(6):496-505.

87. Schmidt-Erfurth U, Chong V, Loewenstein A, Larsen M, Souied E, Schlingemann R, Eldem B, Monés J, Richard G, Bandello F, Specialists ESoR. Guidelines for the management of neovascular age-related macular degeneration by the European Society of Retina Specialists (EURETINA). Br J Ophthalmol. 2014;98(9):1144-67.

88. Peres MB, Kato RT, Kniggendorf VF, Cole ED, Onal S, Torres E, Louzada R, Belfort R, Duker JS, Novais EA, Regatieri CV. Comparison of Optical Coherence Tomography Angiography and Fluorescein Angiography for the Identification of Retinal Vascular Changes in Eyes With Diabetic Macular Edema. Ophthalmic Surg Lasers Imaging Retina. 2016;47(11):1013-9.

89. Henke S, Papapostolou I, Heimes B, Lommatzsch A, Pauleikhoff D, Spital G. [OCT-Angiography in diabetic maculopathy : Comparison between microaneurysms and the foveal avascular zone with flourescein angiography]. Ophthalmologe. 2018;115(11):941-7.

90. Eandi CM, Ciardella A, Parravano M, Missiroli F, Alovisi C, Veronese C, Morara MC, Grossi M, Virgili G, Ricci F. Indocyanine Green Angiography and Optical Coherence Tomography Angiography of Choroidal Neovascularization in Age-Related

Macular Degeneration. Investigative ophthalmology & visual science. 2017;58(9):3690-6.

91. Ang M, Cai Y, MacPhee B, Sim DA, Keane PA, Sng CC, Egan CA, Tufail A, Larkin DF, Wilkins MR. Optical coherence tomography angiography and indocyanine green angiography for corneal vascularisation. Br J Ophthalmol. 2016;100(11):1557-63.

92. Zhu L, Bartsch DU, Freeman WR, Sun PC, Fainman Y. Modeling human eye aberrations and their compensation for high-resolution retinal imaging. Optom Vis Sci. 1998;75(11):827-39.

93. Cicinelli MV, Cavalleri M, Consorte AC, Rabiolo A, Sacconi R, Bandello F, Querques G. Swept-source and spectral domain optical coherence tomography angiography versus dye angiography in the measurement of type 1 neovascularization. Retina (Philadelphia, Pa). 2020;40(3):499-506.

94. Costanzo E, Miere A, Querques G, Capuano V, Jung C, Souied EH. Type 1 Choroidal Neovascularization Lesion Size: Indocyanine Green Angiography Versus Optical Coherence Tomography Angiography. Investigative ophthalmology & visual science. 2016;57(9):OCT307-13.

95. Told R, Sacu S, Hecht A, Baratsits M, Eibenberger K, Kroh ME, Rezar-Dreindl S, Schlanitz FG, Weigert G, Pollreisz A, Schmidt-Erfurth U. Comparison of SD-Optical Coherence Tomography Angiography and Indocyanine Green Angiography in Type 1 and 2 Neovascular Age-related Macular Degeneration. Investigative ophthalmology & visual science. 2018;59(6):2393-400.

96. Yu PK, Mehnert A, Athwal A, Sarunic MV, Yu DY. Use of the Retinal Vascular Histology to Validate an Optical Coherence Tomography Angiography Technique. Transl Vis Sci Technol. 2021;10(1):29.

97. Sampson DM, Dubis AM, Chen FK, Zawadzki RJ, Sampson DD. Towards standardizing retinal optical coherence tomography angiography: a review. Light Sci Appl. 2022;11(1):63.

98. Osborne NN, Casson RJ, Wood JP, Chidlow G, Graham M, Melena J. Retinal ischemia: mechanisms of damage and potential therapeutic strategies. Prog Retin Eye Res. 2004;23(1):91-147.

99. Berry D, Thomas AS, Fekrat S, Grewal DS. Association of Disorganization of Retinal Inner Layers with Ischemic Index and Visual Acuity in Central Retinal Vein Occlusion. Ophthalmol Retina. 2018;2(11):1125-32.

100. Balaratnasingam C, Inoue M, Ahn S, McCann J, Dhrami-Gavazi E, Yannuzzi LA, Freund KB. Visual Acuity Is Correlated with the Area of the Foveal Avascular Zone in Diabetic Retinopathy and Retinal Vein Occlusion. Ophthalmology. 2016;123(11):2352-67.

101. Kang JW, Yoo R, Jo YH, Kim HC. Correlation of microvascular structures on optical coherence tomography angiography with visual acuity in retinal vein occlusion. Retina (Philadelphia, Pa). 2017;37(9):1700-9.

102. Bresnick GH, De Venecia G, Myers FL, Harris JA, Davis MD. Retinal ischemia in diabetic retinopathy. Arch Ophthalmol. 1975;93(12):1300-10.

103. Al-Sheikh M, Akil H, Pfau M, Sadda SR. Swept-Source OCT Angiography Imaging of the Foveal Avascular Zone and Macular Capillary Network Density in Diabetic Retinopathy. Investigative ophthalmology & visual science. 2016;57(8):3907-13.

104. Artin E. Geometric Algebra. Hoboken, NJ, USA: John Wiley & Sons; 2011.

105. Schindelin J, Rueden CT, Hiner MC, Eliceiri KW. The ImageJ ecosystem: An open platform for biomedical image analysis. Mol Reprod Dev. 2015;82(7-8):518-29.

106. Early Treatment Diabetic Retinopathy Study Research G. Grading Diabetic Retinopathy from Stereoscopic Color Fundus Photographs - An Extension of the Modified Airlie House Classification: ETDRS Report Number 10. Ophthalmology. 2020;127(4S):S99-S119.

107. Bland JM, Altman DG. Statistical methods for assessing agreement between two methods of clinical measurement. Lancet. 1986;1(8476):307-10.

108. Team RC. *R: A language and environment for statistical computing*. R Foundation for Statistical Computing, Vienna, Austria. 2021 [Available from: https://www.R-project.org/.

109. Dowle M, Srinivasan A. *Data table: Extension of `data.frame`. R package* version 1.14.2. 2021 [Available from: https://CRAN.R-project.org/package=data.table.

110. Lehnert B. *BlandAltmanLeh: Plots (Slightly Extended) Bland-Altman Plots*. R package version 0.3.1. 2015 [Available from: https://CRAN.R-project.org/package=BlandAltmanLeh.

111. Wickham H. ggplot2: Elegant Graphics for Data Analysis.: Springer-Verlag New York; 2016.

112. Kassambara A. *ggpubr: 'ggplot2' Based Publication Ready Plots*. R package version 0.4.0. 2020 [Available from: https://CRAN.R-project.org/package=ggpubr.

113. Ronneberger O FP, Brox T. U-net: Convolutional Networks for Biomedical Image Segmentation Olaf Ronneberger, Philipp Fischer, Thomas Brox. Medical Image Computing and Computer-Assisted Intervention (MICCAI). 2015:234-41.

114. He K GG, Girshick RB. Mask R-CNN. Proc IEEE Int Conf Comput Vis. 2017;3:2961-9.

115. Shamonin DP, Bron EE, Lelieveldt BP, Smits M, Klein S, Staring M, Initiative AsDN. Fast parallel image registration on CPU and GPU for diagnostic classification of Alzheimer's disease. Front Neuroinform. 2013;7:50.

116. Klein S, Staring M, Murphy K, Viergever MA, Pluim JP. elastix: a toolbox for intensity-based medical image registration. IEEE Trans Med Imaging. 2010;29(1):196-205.

117. Schindelin J, Arganda-Carreras I, Frise E, Kaynig V, Longair M, Pietzsch T, Preibisch S, Rueden C, Saalfeld S, Schmid B, Tinevez JY, White DJ, Hartenstein V, Eliceiri K, Tomancak P, Cardona A. Fiji: an open-source platform for biological-image analysis. Nat Methods. 2012;9(7):676-82.

118. Lin A, Fang D, Li C, Cheung CY, Chen H. Improved Automated Foveal Avascular Zone Measurement in Cirrus Optical Coherence Tomography Angiography Using the Level Sets Macro. Transl Vis Sci Technol. 2020;9(12):20.

119. Stanga PE, Tsamis E, Papayannis A, Stringa F, Cole T, Jalil A. Swept-Source Optical Coherence Tomography Angio™ (Topcon Corp, Japan): Technology Review. Developments in ophthalmology. 2016;56:13-7.

120. Sun JK, Lin MM, Lammer J, Prager S, Sarangi R, Silva PS, Aiello LP. Disorganization of the retinal inner layers as a predictor of visual acuity in eyes with center-involved diabetic macular edema. JAMA ophthalmology. 2014;132(11):1309-16.

121. Boom J, Visser LH. Quantitative assessment of nerve echogenicity: Comparison of methods for evaluating nerve echogenicity in ulnar neuropathy at the elbow. Clin Neurophysiol. 2012;123(7):1446-53.

122. Kaur R, LeAnder R, Mishra NK, Hagerty JR, Kasmi R, Stanley RJ, Celebi ME, Stoecker WV. Thresholding methods for lesion segmentation of basal cell carcinoma in dermoscopy images. Skin Res Technol. 2017;23(3):416-28.

123. Cole ED, Ferrara D, Novais EA, Louzada RN, Waheed NK. Clinical trial endpoints for optical coherence tomography angiography in neovascular age-related macular degeneration. Retina (Philadelphia, Pa). 2016;36 Suppl 1:S83-S92.

124. Garrity ST, Sarraf D. The Arc of Change in Optical Coherence Tomographic Angiography Technology: Progression Toward Greater Reliability. JAMA ophthalmology. 2017;135(10):1098-9.

125. Lei J, Durbin MK, Shi Y, Uji A, Balasubramanian S, Baghdasaryan E, Al-Sheikh M, Sadda SR. Repeatability and Reproducibility of Superficial Macular Retinal Vessel Density Measurements Using Optical Coherence Tomography Angiography En Face Images. JAMA ophthalmology. 2017.

126. Al-Sheikh M, Tepelus TC, Nazikyan T, Sadda SR. Repeatability of automated vessel density measurements using optical coherence tomography angiography. Br J Ophthalmol. 2017;101(4):449-52.

127. Manalastas PIC, Zangwill LM, Saunders LJ, Mansouri K, Belghith A, Suh MH, Yarmohammadi A, Penteado RC, Akagi T, Shoji T, Weinreb RN. Reproducibility of Optical Coherence Tomography Angiography Macular and Optic Nerve Head Vascular Density in Glaucoma and Healthy Eyes. J Glaucoma. 2017;26(10):851-9.

128. Munk MR, Kashani AH, Tadayoni R, Korobelnik JF, Wolf S, Pichi F, Tian M. Standardization of OCT Angiography Nomenclature in Retinal Vascular Diseases: First Survey Results. Ophthalmol Retina. 2021;5(10):981-90.

129. Tan B, Sim YC, Chua J, Yusufi D, Wong D, Yow AP, Chin C, Tan ACS, Sng CCA, Agrawal R, Gopal L, Sim R, Tan G, Lamoureux E, Schmetterer L. Developing a

normative database for retinal perfusion using optical coherence tomography angiography. Biomed Opt Express. 2021;12(7):4032-45.

130. Monares-Zepeda G, Montano M, Bonilla LA, Chew-Bonilla A, Lima-Gómez V. Vessel/perfusion density in two optical coherence tomographic angiography protocols: Interchangeable? Gac Med Mex. 2021;157(2):160-6.

131. Yannuzzi LA, Rohrer KT, Tindel LJ, Sobel RS, Costanza MA, Shields W, Zang E. Fluorescein angiography complication survey. Ophthalmology. 1986;93(5):611-7.

132. Takayama K, Ito Y, Kaneko H, Kataoka K, Sugita T, Maruko R, Hattori K, Ra E, Haga F, Terasaki H. Comparison of indocyanine green angiography and optical coherence tomographic angiography in polypoidal choroidal vasculopathy. Eye (Lond). 2017;31(1):45-52.

133. Novais EA, Adhi M, Moult EM, Louzada RN, Cole ED, Husvogt L, Lee B, Dang S, Regatieri CV, Witkin AJ, Baumal CR, Hornegger J, Jayaraman V, Fujimoto JG, Duker JS, Waheed NK. Choroidal Neovascularization Analyzed on Ultrahigh-Speed Swept-Source Optical Coherence Tomography Angiography Compared to Spectral-Domain Optical Coherence Tomography Angiography. Am J Ophthalmol. 2016;164:80-8.

134. Miller AR, Roisman L, Zhang Q, Zheng F, Rafael de Oliveira Dias J, Yehoshua Z, Schaal KB, Feuer W, Gregori G, Chu Z, Chen CL, Kubach S, An L, Stetson PF, Durbin MK, Wang RK, Rosenfeld PJ. Comparison Between Spectral-Domain and Swept-Source Optical Coherence Tomography Angiographic Imaging of Choroidal Neovascularization. Investigative ophthalmology & visual science. 2017;58(3):1499-505.

135. Littmann H. [Determination of the real size of an object on the fundus of the living eye]. Klin Monbl Augenheilkd. 1982;180(4):286-9.

136. Dai Y, Xin C, Zhang Q, Chu Z, Zhou H, Zhou X, Qiao L, Wang RK. Impact of ocular magnification on retinal and choriocapillaris blood flow quantification in myopia

with swept-source optical coherence tomography angiography. Quant Imaging Med Surg. 2021;11(3):948-56.

137. Kropp M, Golubnitschaja O, Mazurakova A, Koklesova L, Sargheini N, Vo TKS, de Clerck E, Polivka J, Potuznik P, Stetkarova I, Kubatka P, Thumann G. Diabetic retinopathy as the leading cause of blindness and early predictor of cascading complications-risks and mitigation. EPMA J. 2023;14(1):21-42.

138. Klein BE. Overview of epidemiologic studies of diabetic retinopathy. Ophthalmic Epidemiol. 2007;14(4):179-83.

139. Hwang TS, Jia Y, Gao SS, Bailey ST, Lauer AK, Flaxel CJ, Wilson DJ, Huang D. Optical coherence tomography angiography features of diabetic retinopathy. Retina (Philadelphia, Pa). 2015;35(11):2371-6.

140. Hwang TS, Gao SS, Liu L, Lauer AK, Bailey ST, Flaxel CJ, Wilson DJ, Huang D, Jia Y. Automated Quantification of Capillary Nonperfusion Using Optical Coherence Tomography Angiography in Diabetic Retinopathy. JAMA ophthalmology. 2016;134(4):367-73.

141. Ishibazawa A, Nagaoka T, Takahashi A, Omae T, Tani T, Sogawa K, Yokota H, Yoshida A. Optical Coherence Tomography Angiography in Diabetic Retinopathy: A Prospective Pilot Study. Am J Ophthalmol. 2015;160(1):35-44.e1.

142. Jia Y, Bailey ST, Hwang TS, McClintic SM, Gao SS, Pennesi ME, Flaxel CJ, Lauer AK, Wilson DJ, Hornegger J, Fujimoto JG, Huang D. Quantitative optical coherence tomography angiography of vascular abnormalities in the living human eye. Proceedings of the National Academy of Sciences of the United States of America. 2015;112(18):E2395-402.

143. Matsunaga DR, Yi JJ, De Koo LO, Ameri H, Puliafito CA, Kashani AH. Optical Coherence Tomography Angiography of Diabetic Retinopathy in Human Subjects. Ophthalmic Surg Lasers Imaging Retina. 2015;46(8):796-805.

144. de Carlo TE, Bonini Filho MA, Baumal CR, Reichel E, Rogers A, Witkin AJ, Duker JS, Waheed NK. Evaluation of Preretinal Neovascularization in Proliferative Diabetic Retinopathy Using Optical Coherence Tomography Angiography. Ophthalmic Surg Lasers Imaging Retina. 2016;47(2):115-9.

145. Kashani AH, Lee SY, Moshfeghi A, Durbin MK, Puliafito CA. Optical coherence tomography angiography of retinal venous occlusion. Retina (Philadelphia, Pa). 2015;35(11):2323-31.

146. Rispoli M, Savastano MC, Lumbroso B. Capillary network anomalies in branch retinal vein occlusion on optical coherence tomography angiography. Retina (Philadelphia, Pa). 2015;35(11):2332-8.

147. Adhi M, Filho MA, Louzada RN, Kuehlewein L, de Carlo TE, Baumal CR, Witkin AJ, Sadda SR, Sarraf D, Reichel E, Duker JS, Waheed NK. Retinal Capillary Network and Foveal Avascular Zone in Eyes with Vein Occlusion and Fellow Eyes Analyzed With Optical Coherence Tomography Angiography. Investigative ophthalmology & visual science. 2016;57(9):OCT486-94.

148. Cuenca N, Ortuño-Lizarán I, Sánchez-Sáez X, Kutsyr O, Albertos-Arranz H, Fernández-Sánchez L, Martínez-Gil N, Noailles A, López-Garrido JA, López-Gálvez M, Lax P, Maneu V, Pinilla I. Interpretation of OCT and OCTA images from a histological approach: Clinical and experimental implications. Prog Retin Eye Res. 2020;77:100828.

149. Takase N, Nozaki M, Kato A, Ozeki H, Yoshida M, Ogura Y. Enlargement of foveal avascular zone in diabetic eyes evaluated by en face optical coherence tomography angiography. Retina (Philadelphia, Pa). 2015;35(11):2377-83.

150. Lammer J, Karst SG, Lin MM, Cheney M, Silva PS, Burns SA, Aiello LP, Sun JK. Association of Microaneurysms on Adaptive Optics Scanning Laser Ophthalmoscopy With Surrounding Neuroretinal Pathology and Visual Function in Diabetes. Investigative ophthalmology & visual science. 2018;59(13):5633-40.

151. Mo B, Zhou HY, Jiao X, Zhang F. Evaluation of hyperreflective foci as a prognostic factor of visual outcome in retinal vein occlusion. Int J Ophthalmol. 2017;10(4):605-12.

152. Bolz M, Schmidt-Erfurth U, Deak G, Mylonas G, Kriechbaum K, Scholda C, Vienna DRRG. Optical coherence tomographic hyperreflective foci: a morphologic sign of lipid extravasation in diabetic macular edema. Ophthalmology. 2009;116(5):914-20.

153. Lee HE, Wang Y, Fayed AE, Fawzi AA. Exploring the relationship between collaterals and vessel density in retinal vein occlusions using optical coherence tomography angiography. PLoS One. 2019;14(7):e0215790.

154. Ghashut R, Muraoka Y, Ooto S, Iida Y, Miwa Y, Suzuma K, Murakami T, Kadomoto S, Tsujikawa A, Yoshimura N. EVALUATION OF MACULAR ISCHEMIA IN EYES WITH CENTRAL RETINAL VEIN OCCLUSION: An Optical Coherence Tomography Angiography Study. Retina (Philadelphia, Pa). 2018;38(8):1571-80.

155. Scarinci F, Varano M, Parravano M. Retinal Sensitivity Loss Correlates with Deep Capillary Plexus Impairment in Diabetic Macular Ischemia. J Ophthalmol. 2019;2019:7589841.

156. Pereira F, Godoy BR, Maia M, Regatieri CV. Microperimetry and OCT angiography evaluation of patients with ischemic diabetic macular edema treated with monthly intravitreal bevacizumab: a pilot study. Int J Retina Vitreous. 2019;5:24.

9. Bibliography of the candidate's publications

9.1. Publications related to the PhD thesis

1. **Orsolya Angeli**, Dorottya Hajdu, Aniko Jeney, Balint Czifra, Balazs Vince Nagy, Tamas Balazs, Dora Jakaboczkine Nemoda, Gabor Mark Somfai, Zoltan Z. Nagy, Tunde Peto & Miklos Schneider. Qualitative and quantitative comparison of two semi-manual retinal vascular density analyzing methods on optical coherence tomography angiography images of healthy individuals. Sci Rep, 2023. **13**(1): p. 16981 **IF: 4,6**

2. Reinhard Told, Gregor S. Reiter, **Orsolya Angeli**, Tamara J. Mittermüller, Katharina Eibenberger, Ferdinand G. Schlanitz, Mustafa Afrikan, Andreas Pollreisz, Stefan Sacu, Ursula Schmidt-Erfurth. Swept source optical coherence tomography angiography, fluorescein angiography, and indocyanine green angiography comparisons revisited: Using a Novel Deep-Learning-Assisted Approach for Image Registration. Retina, 2020. **40**(10): p. 2010-2017. **IF: 4,256**

3. Dorottya Hajdu, Reinhard Told, **Orsolya Angeli**, Guenther Weigert, Andreas Pollreisz, Ursula Schmidt-Erfurth, Stefan Sacu. Identification of microvascular and morphological alterations in eyes with central retinal non-perfusion. PLoS One, 2020. **15**(11): p. e0241753. **IF: 3,240**

Σ Impact factor: 12,096

9.2. Publications not related to the PhD thesis

1. **Angeli Orsolya**, Veres Dániel Sándor, Nagy Zoltán Zsolt, Schneider Miklós. Az IMEA ADR III kritikus fúziós frekvenciavizsgáló eszközzel végzett mérések reprodukálhatóságának vizsgálata. Orv Hetil, 2016. **157**(27): p. 1079-86. **IF: 0,349**

2. **Angeli Orsolya**, Nagy Zoltán Zsolt, Schneider Miklós. Szemfenéki arteria centralis retinae érelzáródás miatt kialakult hirtelen látásromlás spontán restitúciója cilioretinalis artéria jelenlétében. Orv Hetil, 2019. **160**(29): p. 1146-1152. **IF: 0,497**

3. Miklos Schneider, Adel Molnar, **Orsolya Angeli**, Dorottya Szabo, Fruzsina Bernath, Dorottya Hajdu, Eszter Gombocz, Balint Mate, Balint Jiling, Balazs Vince Nagy, Zoltan Zsolt Nagy, Tunde Peto, Andras Papp. Prevalence of Cilioretinal Arteries: A systematic review and a prospective cross-sectional observational study. Acta Ophthalmol, 2021. **99**(3): p. e310-e318. **IF: 3,988**

4. **Angeli Orsolya**, Nagy Zoltán Zsolt, Schneider Miklós. Felnőttkori B-típusú Niemann–Pick-betegség szemészeti manifesztációja. Orv Hetil. 2023;164(46):1838-44. **IF: 0,6**

DOI:10.14753/SE.2024.3041

10. Acknowledgements

First and foremost, I owe a debt of gratitude to my supervisor, **Dr. Miklós Schneider**, who has been supporting my research for years, allowed me to acquire professional knowledge in ophthalmology, and sparked my interest in scientific research. Without his guidance and encouragement, this Ph.D. study would not have been possible. I am fortunate to have an experienced advisor like him.

I am very grateful for my mentor, **Dr. Tibor Milibák**, who has not only encouraged my scientific aspirations but has also been instrumental in fostering my professional growth as an ophthalmologist. His boundless energy and enthusiasm for the field of ophthalmology have consistently served as a powerful source of motivation for me.

I owe my gratitude to **Prof. Dr. Zoltán Zsolt Nagy and Prof. Dr. Ildikó Süveges**, who allowed me, as Ophthalmology Program coordinator, to study at Károly Rácz Clinical Medicine Doctoral School and supported me by facilitating my research at Semmelweis University Department of Ophthalmology.

I extend a special thank you to **Prof. Dr. Ursula Schmidt-Erfurth** and **Prof. Dr. Stefan Sacu**, for allowing me to participate in an international research group and for recognizing my research work.

Additionally, I extend a special thank you to all of my colleagues at the Department of Ophthalmology of Semmelweis University and at the Department of Ophthalmology, Uzsoki Hospital for their continuous assistance and support.

Last, but not least, I would like to express my heartfelt gratitude for the unwavering support of my family, especially my beloved husband, who provides a constant foundation of support and balance in my life. His patience, motivation, and unwavering faith in my achievements continually served as a wellspring of inspiration throughout this demanding journey.